Manufacturing Rev. **10**, 4 (2023)

https://doi.org/10.1051/mfreview/2023002

**Manufacturing Review**
Available online at:
https://mfr.edp-open.org

RESEARCH ARTICLE OPEN ACCESS

# Effect of $TiO_2$ inoculants on the wear conduct of the aluminium AA 6061/red mud high performance hybrid composite

Niranjan Hugar[1,2,3,*], B. Venkata Narayana [1], Santhosh Nagaraja[2], and Sunil Waddar[2]

[1] Department of Mechanical Engineering, SEA College of Engineering and Technology, Bengaluru 560049, Karnataka, India
[2] Department of Mechanical Engineering, MVJ College of Engineering, Bengaluru 560067, Karnataka, India
[3] Department of Mechanical Engineering, Visvesvaraya Technological University, Belagavi 590018, Karnataka, India

Received: 22 October 2022 / Accepted: 12 January 2023

**Abstract.** The current work focuses on the manufacturing of aluminium AA 6061 composites and its tribological characterization. This is achieved by reinforcing the matrix with red mud. However, the uniform dispersion of red mud requires ultrasonic assisted stir casting and the use of optimum wt.% of $TiO_2$ inoculants. In this regard, the composition of red mud is fixed at 2 wt.%, since the addition of red mud beyond 2 wt.% results in the agglomeration, while the wt.% of $TiO_2$ inoculants is varied from 2 wt.% to 6 wt.%. The wear tests are conducted as per the L9- Orthogonal Array (OA) for a load range of 10 N to 30 N, sliding distance of 500 m to 2500 m, disk rotation speed of 200 RPM to 600 RPM. The regression coefficients are more than 0.9 and close to unity and the error between the experimental outcomes and statistical values are within the tolerance band. The SWR and COF is minimized for 2 wt.% of red mud, 4 wt.% of $TiO_2$, beyond which there is a slight increase in the wear of the composites attributed to the agglomeration of the reinforcments in certain localized regions and the presence of voids in other regions.

**Keywords:** Aluminium AA 6061 / $TiO_2$ / red mud / inoculants / composites / wear / RSM / SWR / COF

## 1 Introduction

The role of aluminium composites in engineering applications have gained significance due to the mutliple advantages it offers. However, the distribution of the reinforcements in the aluminium matrix is one of the drawback, which needs to be overcome. The utilization of inoculants in this regard, can bring about homogeneity in castings [1] and the prerequisite of such composites has achieved the improvement in the different processing methodologies to achieve these gigantic possibilities [2,3]. Stir casting is of major process methodology for fabrication of the composites due to the benefits that the technique acquires contrasted with various manufacture processes, this strategy yields composites with consistent properties. With the improvement in stir casting procedures, a colossal assortment of composites can be developed in contrast to conventional process methodologies. Further, the inoculants have substantial impact on the characteristics and there is a need for effectively studying them. Further, the requirements for high level attributes from the hybrid composites have reiterated the need for the effective utilization of these inoculants in matrix alloy for auto, medical, construction, aviation, and related domains. The reinforcement particulates in the matrix phase needs to be homogeneously distributed because they influence the characteristics of the composites. It is moreover extensively revered that the scale and amount of the reinforcements and the composition of the matrix is an important factor. The ceramic reinforcements scattered in a metallic network will generally offer a best combination of mechanical properties [4]. However, it leads to the embrittlement. Also, the vast majority of the investigations on MMC is centered on reinforcing the ceramic particles in Al-based composites to upgrade mechanical properties through the fusion of ceramic particulates into the metallic lattice. Nonetheless, the use of carbides, borides, oxides of metal inside side the Al metallic grid are achieved by solid bonding between the carbides and framework at above 720 °C, within the sight of degassers which upgrade their solidarity. To overcome these inadequacies, substantial research on the inoculants facilitating uniform distribution are essential. Among various inoculants, $TiO_2$ has extreme lubricity, and bonding capabilities at higher temperatures. Especially, the $TiO_2$ inoculants have greater impact on the uniform distribution of red mud reinforcements is the matrix phase. The utilization of $TiO_2$ as inoculants is in fact essential because of its attributes. Until this point of time, the scope of $TiO_2$ for improved nanophase is still in its incipient stage, and necessitates further researches.

* e-mail: niranjan0364@gmail.com

**Table 1.** Elemental composition obtained from the EDS analysis.

| Element | Mg | Al | Si | Cr | Mn | Fe | Cu | Zn |
|---|---|---|---|---|---|---|---|---|
| Weight % | 1.38 | 93.41 | 1.29 | 0.64 | 0.42 | 1.64 | 0.72 | 0.52 |
| Atomic % | 1.56 | 95.3 | 1.26 | 0.34 | 0.21 | 0.81 | 0.31 | 0.22 |

The red mud on the other hand is a byproduct of bayers process, and the dumping of the redmud is a serious environmental threat, which needs to be addressed with utmost concern. The utilization of this red mud reinforcement in the matrix shall provide a sustainable path for handling this byproduct. However, the uniform distribution of red mud in the matrix is a major concern, which needs to be addressed [5,6]. Several researchers have used SiC coated mild steel stirrer with bow shaped cutting edges in stir casting furnace to distribute the red mud uniformly, but to vain [7–9]. Thus, there is a need for inoculants to accentuate the process of distribution of the reinforcements in the matrix. In this regard, the discoveries of Santhosh et al. have reported that the inoculants in the form of fly ash can be appropriately scattered inside the Al grid, likewise the utilization of the hetero-conglomerates, and the fly ash inoculants can upgrade the bonding between the framework and the fortifications [10]. This advancement has prompted the careful utilization of inoculants, that enhances the bondings between the constituents [11]. The consideration of 2.5 wt.% of Fly Debris in the Al grid composite has improved the bonding strength by 35% in correlation with the Al base metal and also a 15.6% reduction in wear rate of the composites [12]. Also, the inoculants significantly influence the hardness and impact strength characteristics of the composites [13–15]. Rana et al. [16] have done broad work on the combination and portrayal of Al network composites and have detailed that the ceramic reinforcements significantly affect the performance of the composites in light of the embrittlement. Al Rubaie et al. [17] have reported their findings on the wear characteristics of Al lattice composites and described that the inclusion of the carbide reinforcements leads to increased resistance to the wear of the composites due to the formation of Al–C bonds and orowan strengthening at the nuclear level. Further, it is important to validate the results of the experiments statistically and Sahin et al. [18] have achieved this by comparing the factual investigations through Taguchi procedures and have highlighted that the optimization of the process parameters significantly affect the wear in the composite specimens. Thus, the use of the inoculants and the optimization of the process parameters in tribological experiments shall reduce the wear and the consideration of ideal measure of fortifications shall result in greater bonding in the composite. The improvement in the process parameters for experimental trials exceptionally improves the wear conduct of the composites [19–22]. In this manner, various scientists have reiterated the importance of the use of suitable inoculants and optimization studies for better tribological performance of the composites [23–25]. Hence, the rationale of the present work is to study the wear conduct of AA 6061/$TiO_2$/red mud composites and to gather a data set for statistical validation of the wear experiments by response surface method based optimization techniques and analyze the influence of the $TiO_2$ inoculants on the tribological characteristics of the composites.

## 2 Materials and methods

### 2.1 Materials

In the present work, aluminium AA 6061 matrix is chosen, as it is used for automotive applications and has excellent formability, weldability, and posses greater strength, corrosion resistance and can be easily forged into required shape and size. The aluminium AA 6061 has Si and Mg as the major alloying elements and can readily bond with the reinforcements. Table 1 gives the composition of the aluminium AA 6061 matrix alloy obtained from the EDS, while Figure 1 gives the EDS of the As cast aluminium AA 6061 alloy. The EDS analysis ascertains the presence of Si and Mg as the major alloying elements, as is the case with the compositional specifications given by the Aluminium Association for 6061 grade alloy. Table 2 gives the properties of the AA 6061 alloy as provided by the supplier data sheet [PMC Metal Corporation, Bengaluru, Karnataka].

The red mud is sourced from National Aluminium Company (NALCO), Gujarat and SEM characterization are accomplished to validate the size and shape of the red mud particles, and the EDS is done to confirm the composition of compounds present in redmud. Figure 2 gives the SEM image of the red mud particles, while Figure 3 gives the EDS analysis of the redmud sample. The size of the red mud particles are found to be in the range of 2–5 μm, with random shapes.

The EDS spectrum distinctly identifies the presence of the oxides of Al, Fe and Si with traces of Ti, which forms the composition of the redmud. The ceramic compounds in the red mud tend to impart better wear resistance, when mixed with the AA 6061 matrix in suitable proportions in the composite.

The $TiO_2$ is sourced from NIMCO metals, Bengaluru and the SEM characterization is done to validate the size and shape of the particulates. Figure 4 gives the SEM image of the $TiO_2$ particles. The size of the the $TiO_2$ particles is found to be 2–10 μm, with tetragonal shapes.

### 2.2 Casting and specimen preparation

The weighed proportions of the Aluminium AA 6061 alloy pieces are fed to the crucible of stir casting furnace, and melted at a temperature of 690 °C in inert gas environment to prevent the atmospheric oxygen from getting entrapped in the molten metal. The degassing tablets (hexachloroethane)

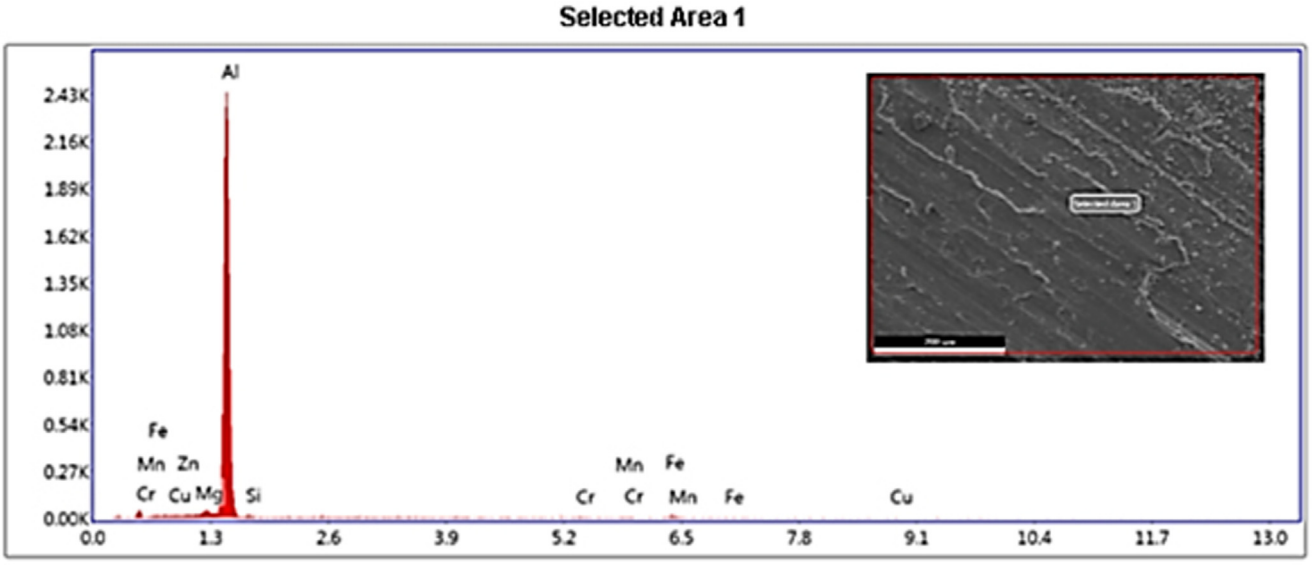


**Fig. 1.** EDS spectrum of As cast Aluminium AA 6061 alloy.

**Table 2.** Property table provided by the supplier data sheet.

| Property | Value |
|---|---|
| Density | 2.7 g/cm$^3$ |
| Brinell hardness | 95 BHN |
| Ultimate tensile strength | 310 MPa |
| Yield strength | 276 MPa |
| Youngs modulus | 68.9GPa |
| Coefficient of thermal expansion | 23.6 μm/m°C |
| Thermal conductivity | 167 W/mK |

are dropped into the molten metal to remove the oxides and allied impurities, which form the slag that is skimmed off from the surface of the molten metal. Post removal of the slag from the molten metal, the weighed proportions of preheated $TiO_2$ and red mud reinforcements along with 0.5 g of Mg wrapped in an aluminium foil are introduced into the molten metal and the mixture is heated to a temperature of 720 °C and then stirred continuously at a speed of 500 rpm for two stretches of 10 min duration each. Subsequently, one more round of degassing is carried out by the addition of coverall flux, followed by the removal of slag from the surface of the molten metal. The wt.% of red mud is kept constant at 2 wt. %, while the composition of the $TiO_2$ inoculants are varied from 2 wt.% to 6 wt.%. The composition of the reinforcements are considered based on the existing literature review and the initial set of pilot experiments before actual research experimentations. The addition of the red mud beyond 2 wt. % will cause agglomeration and will subsequently come out in the form of slag, when the flux is added. This is the main hindrance which is limiting the red mud composition in the matrix. Also, Santhosh et al. [26], have reported that the increase in the reinforcements beyond 10 wt.% shall result in agglomeration of the reinforcements in the matrix thereby causing inhomogeneous distribution of the particulates and void formations in certain localized regions. Table 3 gives the composition of the matrix and reinforcements in the composites fabricated in the present work.

The castings are then machined to dimensions in accordance with the ASTM G99-95a test standards. The diameter of the specimens is considered as 8 mm, while the length of the specimens is considered as 30 mm. Figure 5 gives the schematic of the pin on disc test specimen.

### 2.3 Experimental

The wear tests are accomplished in accordance with the ASTM G99-95a test standards on a Ducom make ED-201 tribometer. The test parameters for the wear characterization are selected based on the existing literature review and the initial set of pilot trials carried out. The design of experiments for accomplishing the wear tests are done as per the L9 orthogonal array (OA) with the loads considered for the experimental trials ranging from 10 N to 30 N with an interval of 10 N between each of the trials, sliding distance ranging from 500 to 2500 m with an interval of 1000 m between each of the trials, disk rotation speed ranging from 200 to 600 rpm with an interval of 200 rpm between each of the trials. The pin on disc specimens are clamped against a rotating EN 32 grade steel disc, and the experiments are conducted. The Friction Force (FF) and the Coefficient of Friction (COF) are recorded for each of the trials from equation (1). Further, the loss of the volume due to the wear is determined by subtracting the volume of the specimen after wear from the initial volume of the specimen. This magnitude of volume loss is further used for calculating the specific wear rate (SWR) using the equation (2), in accordance with the ASTM G99-05 standards [26–30]. The Response Surface Methodology (RSM) optimization studies are further carried out on the

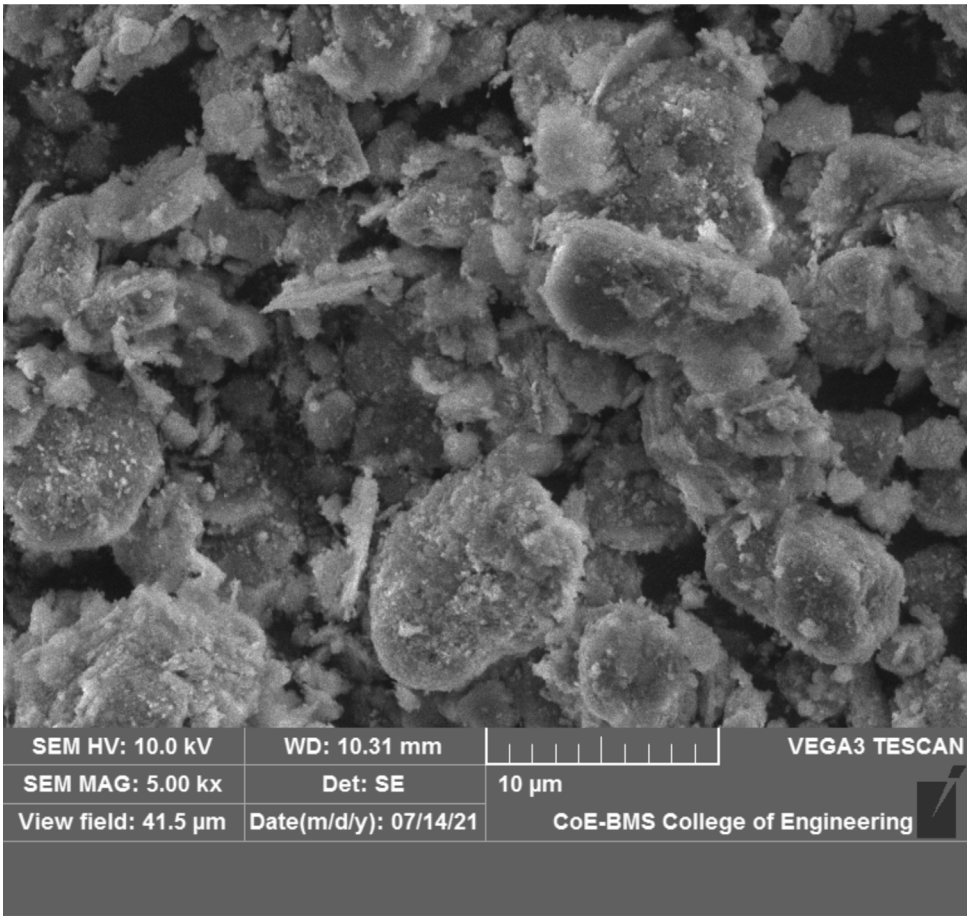


**Fig. 2.** SEM image of red mud particles.

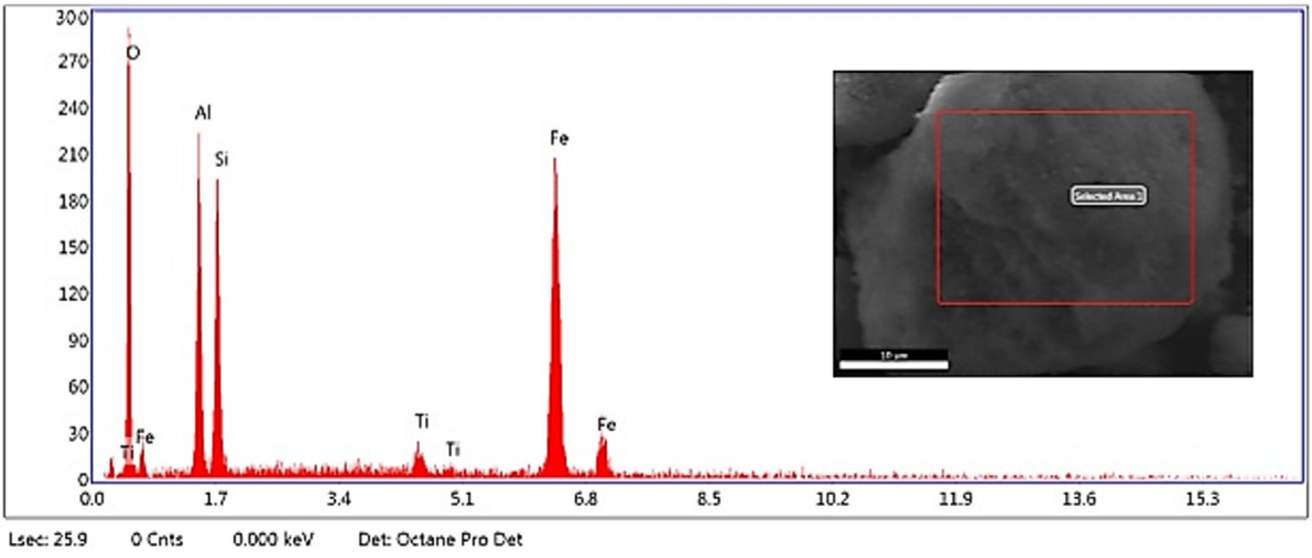


**Fig. 3.** EDS spectrum of red mud particles.

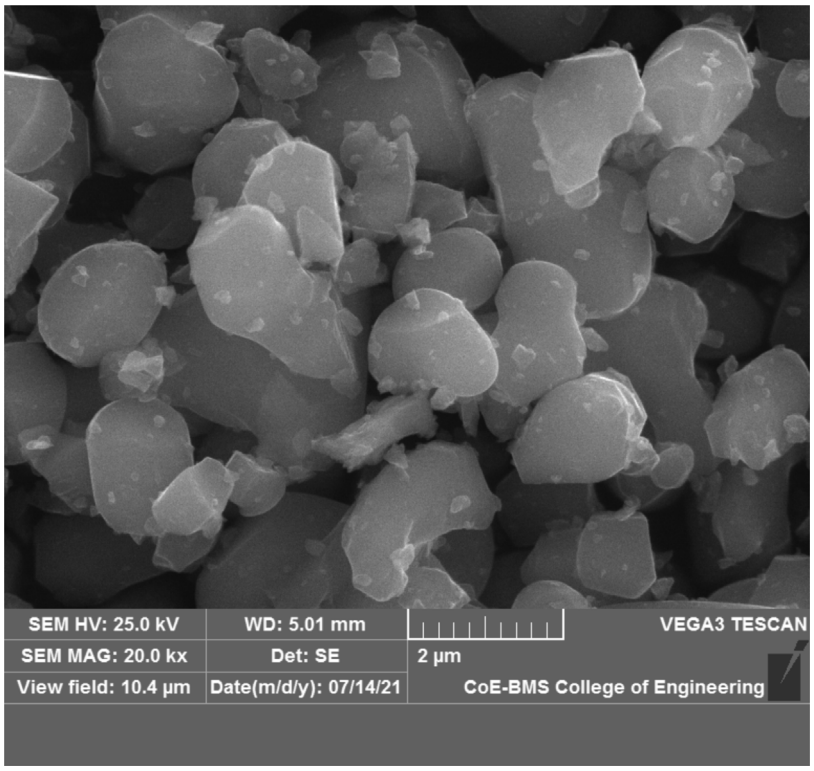


**Fig. 4.** SEM image of $TiO_2$ particles.

**Table 3.** Composition of composite specimens.

| Composition | wt.% of red mud | wt.% of $TiO_2$ | wt.% of AA 6061 |
|---|---|---|---|
| AS CAST | 0 | 0 | 100 |
| AR2T2 | 2 | 2 | 96 |
| AR2T4 | 2 | 4 | 94 |
| AR2T6 | 2 | 6 | 92 |

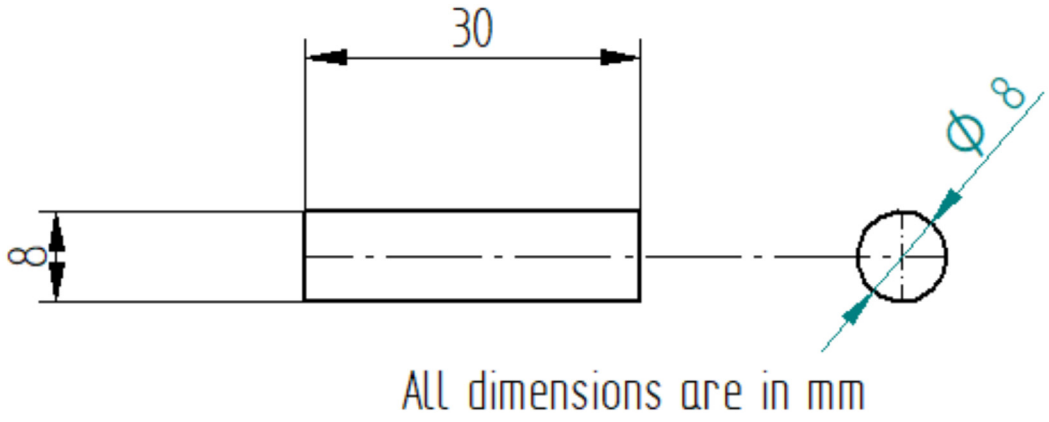


**Fig. 5.** Sketch of the pin on the disc specimen.

**Table 4.** Factors and their levels used for the wear.

| Level | Load (X) in N | Sliding distance [Y] in m | Disk rotation [Z] in RPM |
|---|---|---|---|
| 1 | 10 | 500 | 200 |
| 2 | 20 | 1500 | 400 |
| 3 | 30 | 2500 | 600 |

**Table 5.** Wear results for As cast specimen.

| Run No. | Load (N) | Sliding distance (m) | Disk rotation (rpm) | SWR ($mm^3$/Nm) | COF |
|---|---|---|---|---|---|
| 1 | 10 | 500 | 200 | 0.00626 | 0.339 |
| 2 | 10 | 1500 | 400 | 0.00562 | 0.354 |
| 3 | 10 | 2500 | 600 | 0.00514 | 0.366 |
| 4 | 20 | 500 | 400 | 0.00568 | 0.351 |
| 5 | 20 | 1500 | 600 | 0.00531 | 0.363 |
| 6 | 20 | 2500 | 200 | 0.00422 | 0.376 |
| 7 | 30 | 500 | 200 | 0.00453 | 0.362 |
| 8 | 30 | 1500 | 400 | 0.00359 | 0.389 |
| 9 | 30 | 2500 | 600 | 0.00275 | 0.411 |

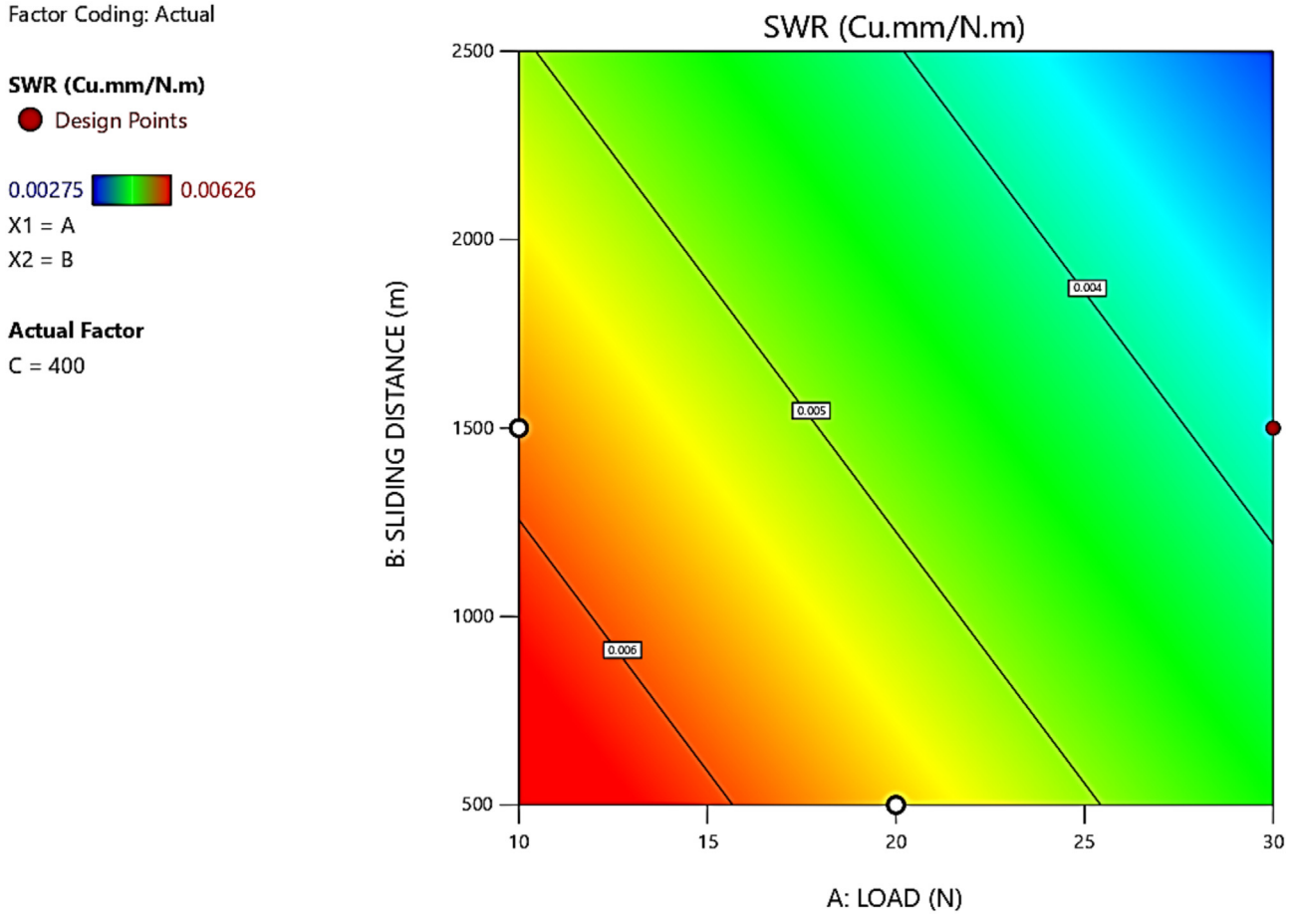


**Fig. 6.** Surface plot for variation of wear with load and sliding distance.

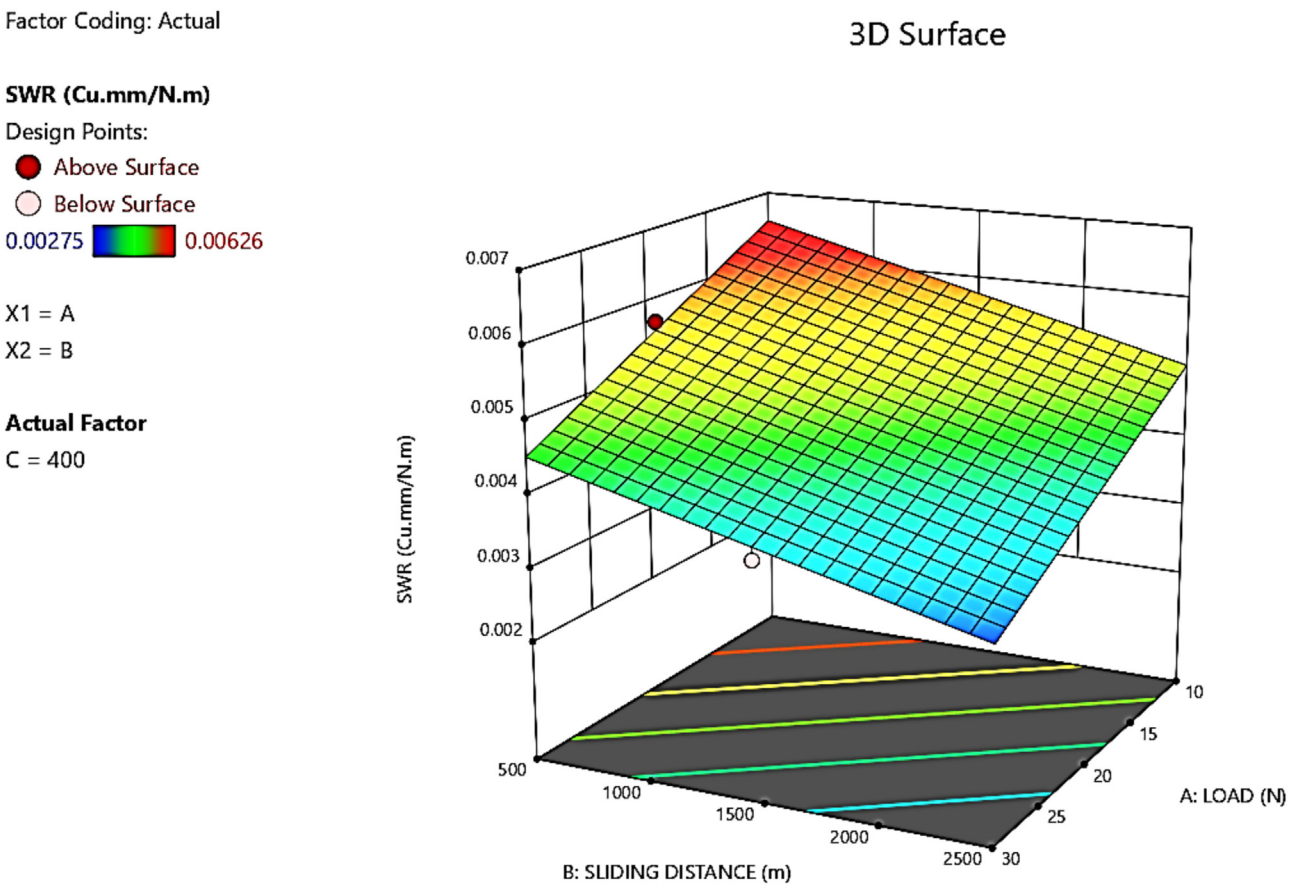


**Fig. 7.** Surface plot for variation of s with load and sliding distance.

**Table 6.** Fit statistics of wear test for As cast specimen.

| | | | |
|---|---|---|---|
| Std. Dev. | 0.0003 | $R^2$ | 0.9475 |
| Mean | 0.0048 | Adjusted $R^2$ | 0.9160 |
| C.V.% | 6.78 | Predicted $R^2$ | 0.7123 |
| | | Adeq precision | 15.8148 |

COF and SWR values to optimize the process parameters post experimental trials. The statistical outcomes and the experimental values are further validated and the error predictions are accomplished to study the influence of process parameters on the wear rate for each of the composite specimens. Subsequently the surface morphology of the worn surfaces are characterized from Scanning Electron Microscopy and the wear debris are effectively studied to understand the wear mechanism [26]

$$\text{Coefficient of Friction } [COF(\mu)] = \frac{F}{N} \tag{1}$$

where F is the frictional, and N is the normal force [26].

$$\text{Specific Wear Rate(SWR)} = \frac{\text{Wear Volume Loss in mm}^3}{(\text{Sliding distance in} m \times \text{Applied Load in} N)} \tag{2}$$

where, wear volume loss is given by $V_{\text{Loss}} = \frac{\pi \times d^2}{4} \times (\text{Wear loss in mm})$; $d$ is the diameter of the pin specimen in mm.

## 2.4 Response surface methodology (RSM) studies

The RSM studies are accomplished to optimize and statistically validate the experimental outcomes. The COF and SWR are validated by considering the three process parameters of the wear experimentations viz., the load ($X$) in N, sliding distance ($Y$) in m and the disk rotation ($Z$) in RPM and modelled for the response optimization based on the three factor approach. Equation (3) gives the response as a function of the process parameters.

$$\lambda = f(X, Y \cdot Z) \tag{3}$$

where λ is the response viz., COF and SWR modeled as a function of the factors $X$, $Y$ and $Z$.

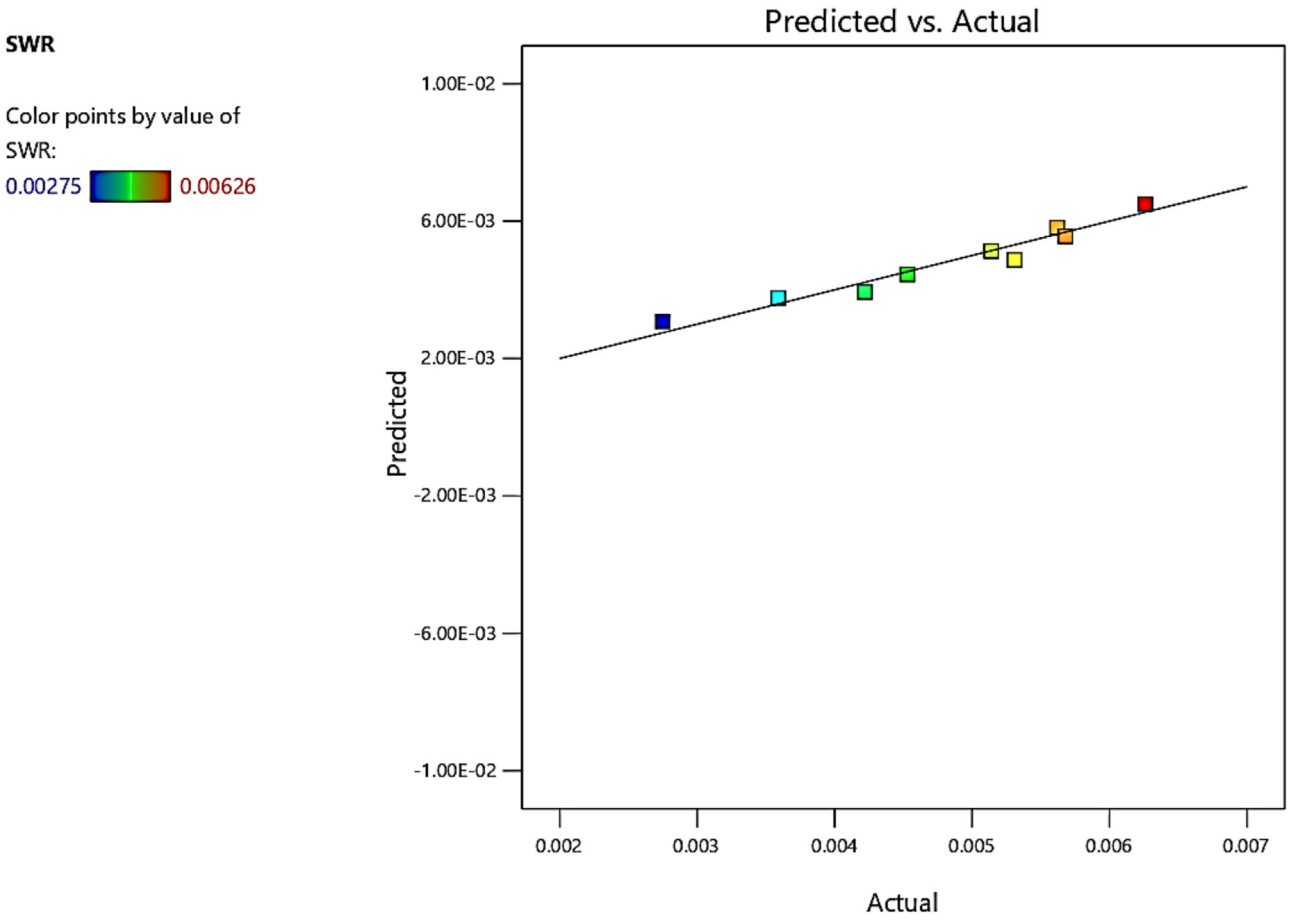


**Fig. 8.** Curve fitting for predicted versus actual values for SWR for As cast specimen.

Further, the regression equations are modelled by considering the three factors and three levels for each of the factors as in Table 4. The experimental outcomes are statistically validated by considering the coefficient of correlation ($R^2$), adjusted $R^2$ and predicted $R^2$ values. The contour plots and surface plots obtained give the variation of the responses for the different factorial levels.

The experimental outcomes obtained as per the L9 orthogonal array are statistically validated using the RSM. From the statistical comparisons, the critical factors are identified and the optimization studies are accomplished.

### 2.5 Scanning electron microscopy (SEM)

The scanning electron microscopy is accomplished using a VEGA 3 TESCAN LMU machine in the Materials Centre of Excellence at BMS College of Engineering at a scanning voltage of 25 kV, with a resolution range of 3.1 nm to 15.5 nm, magnification range of 4.5 X to 1,000,000 X and a five axes control.

The microstructural evaluation gives information about the wear mechanism, morphology of the wear track and the surface characteristics of the worn surfaces [27–32]. The wear track analysis provides a base for evaluating the contact mechanics during the adhesive wear process [33–36].

## 3 Results

### 3.1 Effect of the different factors on COF and SWR for As cast specimen

The pin on disc wear test is carried out on a Ducom make ED-201 tribometer in a controlled environment. The dataset for Friction Force for different factorial levels for a run time of 600 seconds are acquired using a data acquisition system interfaced with the computer. The COF and the SWR for different factorial levels are subsequently computed and tabulated. The outcomes of the experiments are used for statistical modelling using RSM and validated. The results of the experiments for As cast specimen are given in Table 5.

#### 3.1.1 Statistical validation of SWR for As cast specimen

The statistical validation of the wear results are accomplished by the RSM techniques and the surface and 3D contour plots are obtained. Subsequently the analysis of variance (ANOVA) is carried out to seperate observed data and gain sufficient knowledge about the relationship between the dependent and independent variables in the wear test.

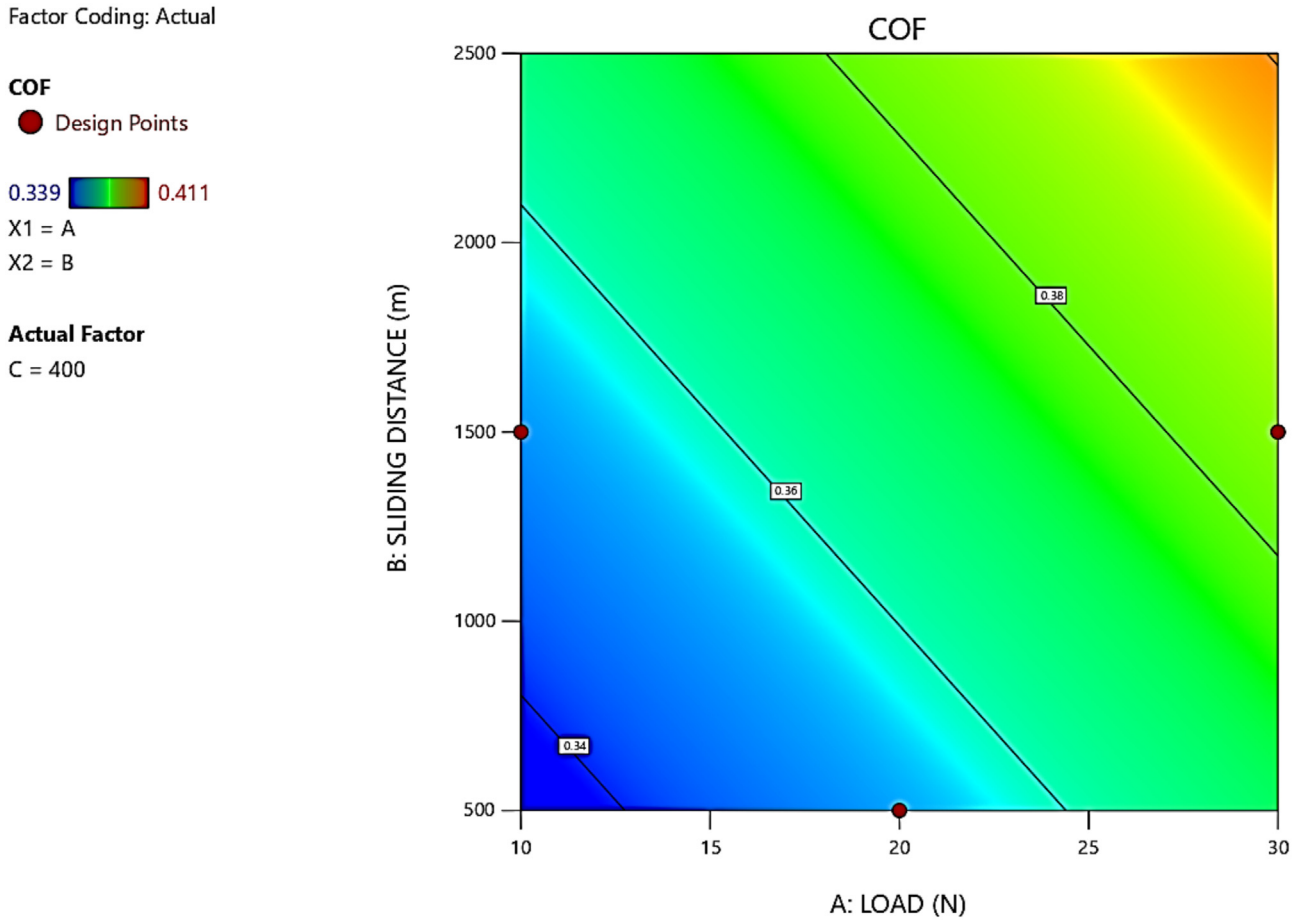


**Fig. 9.** Surface plot for variation of COF with load and sliding distance for As cast specimen.

Figure 6 gives the surface plot, while Figure 7 gives the 3D contour plots for SWR. From, the surface and 3D contour plot, it is evident that the SWR reduces with the increment in the load and the sliding distance.

Further, the regression correlation gives the fit data (Tab. 6) and the plot for curve fitting the predicted versus actual data (Fig. 8). While the equation (4) gives the regression equation from the RSM model for the SWR values obtained using the Design Expert Software.

The $R^2$, Adjusted $R^2$ values are 0.9475 and 0.9160 respectively. This indicates that the coefficient of correlation is close to 1 and the predicted values have a linear fit with the experimental values, with relatively lesser number of outliers.

Adeq Precision measures the signal to noise ratio. A ratio greater than 4 is desirable. In the present work, a ratio of 15.815 indicates an adequate signal. This model can be used to navigate the design space.

$$\begin{aligned}\text{SWR} = {} & +0.007826 - 0.000102 * \text{LOAD} - 7.678E-7 \\ & * \text{SLIDING DISTANCE} + 4.111E-7 \\ & * \text{DISK ROTATION}. \end{aligned} \quad (4)$$

### 3.1.2 Statistical validation of COF for As cast specimen

Figure 9 gives the surface plot, while Figure 10 gives the 3D contour plots for COF. From, the surface and 3D contour plot, it is evident that the COF increases with the increment in the load and the sliding distance.

Further, the regression correlation gives the fit data (Tab. 7) and the plot for curve fitting the predicted versus actual data (Fig. 11). While the equation (5) gives the regression equation from the RSM model for the SWR values obtained using the Design Expert Software. The increase in the COF increases the wear loss, however reduces the SWR, due to the fact that the volumetric wear loss is relatively lesser as compared to the subsequent increase in the load and the sliding distance.

The predicted $R^2$ of 0.6947 is not as close to the adjusted $R^2$ of 0.8967 as one might normally expect; i.e. the difference is more than 0.2. This may indicate a large block effect or a possible problem with the model and/or data. Things to consider are model reduction, response transformation, outliers, etc. All empirical models are tested by doing confirmation runs.

Adeq Precision measures the signal to noise ratio. A ratio greater than 4 is desirable. The ratio of 15.266 indicates an adequate signal. This model can be used to navigate the design space.

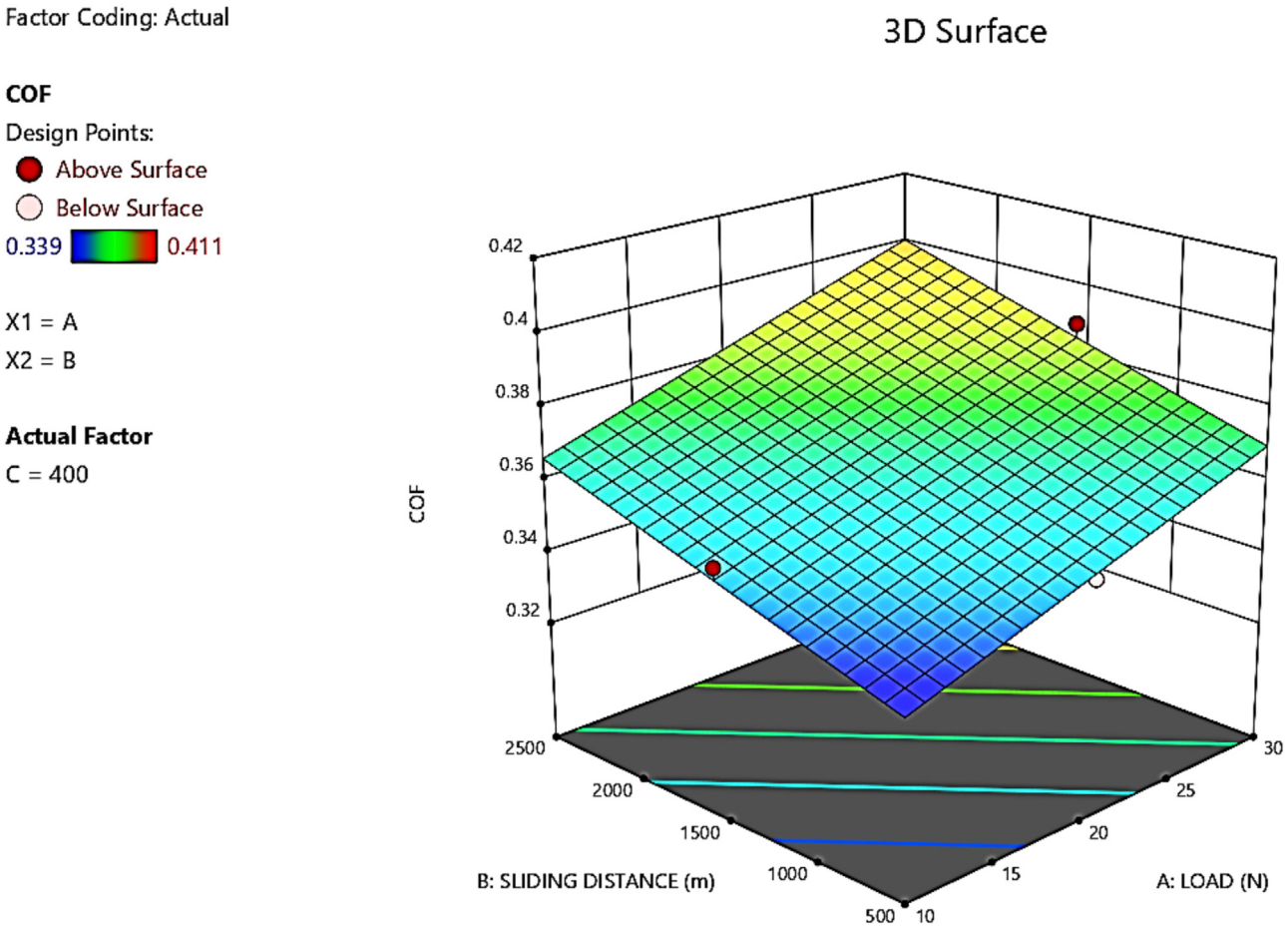


**Fig. 10.** 3D contour plot for variation of COF with load and sliding distance for As cast specimen.

**Table 7.** Fit statistics of wear test for As cast specimen.

| | | | |
|---|---|---|---|
| Std. Dev. | 0.0070 | $R^2$ | 0.9354 |
| Mean | 0.3679 | Adjusted $R^2$ | 0.8967 |
| C.V.% | 1.89 | Predicted $R^2$ | 0.6947 |
| | | Adeq precision | 15.2656 |

$$\text{COF} = +0.304833 + 0.001717 * \text{LOAD} + 0.000015 * \text{SLIDING DISTANCE} + 0.000014 * \text{DISK ROTATION}. \quad (5)$$

### 3.1.3 Analysis of variance (ANOVA) for As cast specimen

Table 8 gives the ANOVA results for SWR for the As Cast Specimens. The Model $F$-value of 30.08 implies the model is significant. There is only a 0.13% chance that an $F$-value this large could occur due to noise.

$P$-values less than 0.0500 indicate model terms are significant. In this case A-Load, and B-Sliding Distance are significant model terms. Values greater than 0.1000 indicate the model terms are not at all significant. Thus, the model term C-Disk Rotation is not having much of the significance on the outcomes of the experiment.

Table 9 gives the ANOVA results for COF. The Model $F$-value of 24.14 implies the model is significant. There is only a 0.21% chance that an $F$-value this large could occur due to noise.

$P$-values less than 0.0500 indicate model terms are significant. In this case A, B are significant model terms. Values greater than 0.1000 indicate the model terms are not significant. Thus, from the model summary, it is evident that the load and sliding distance are having substantial influence on the wear results.

## 3.2 Effect of the different factors on COF and SWR for AR2T2 SPECIMEN

The effect of different set of factors on the COF and SWR are also evaluated for the AR2T2 specimen. The wear results are tabulated in Table 10.

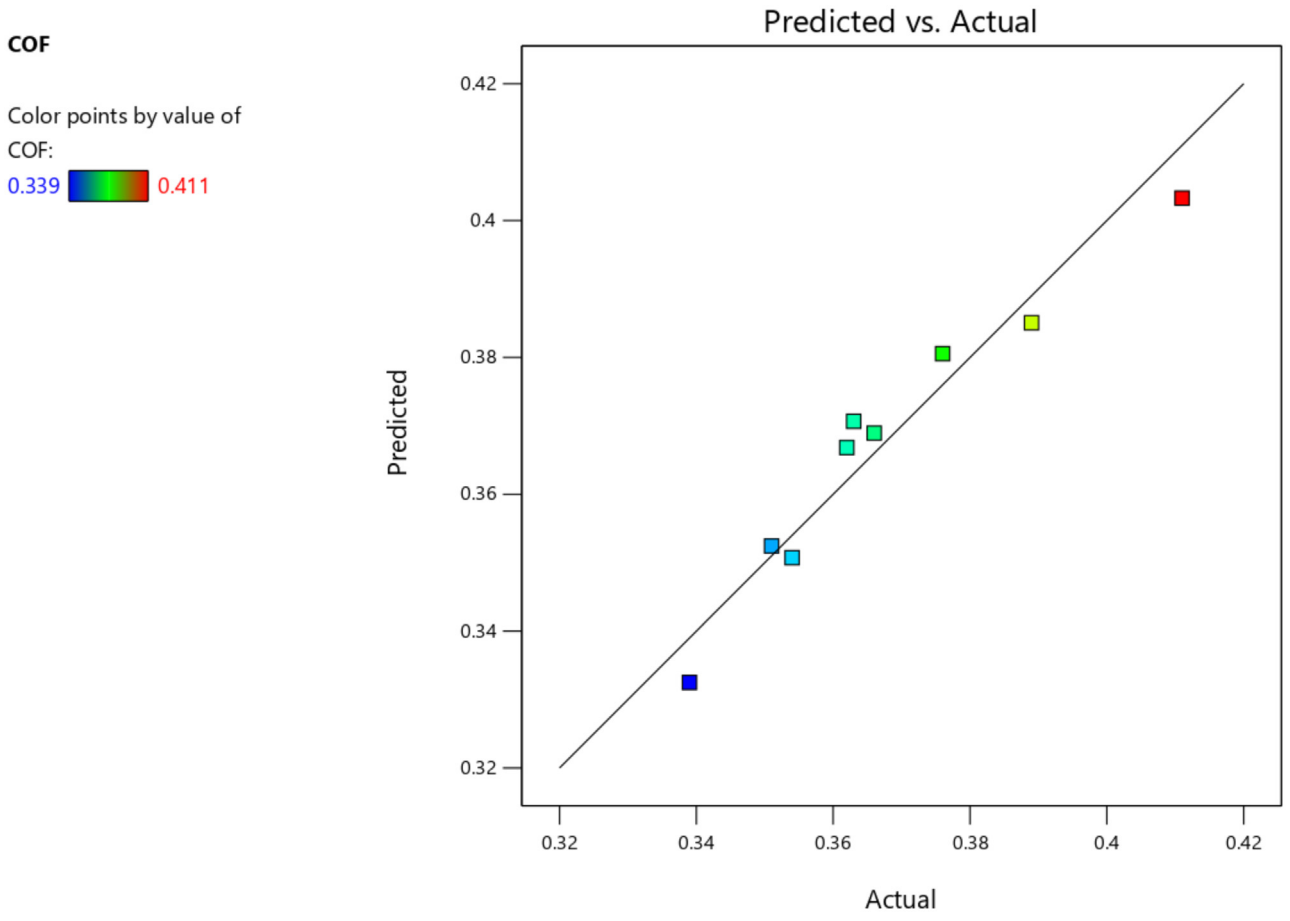


**Fig. 11.** Curve fitting for Predicted vs. Actual values for COF for As Cast specimen.

**Table 8.** ANOVA table for SWR for As cast specimens.

| Source | Sum of squares | df | Mean square | *F*-value | *p*-value | Remarks |
|---|---|---|---|---|---|---|
| Model | 9.502E–06 | 3 | 3.167E–06 | 30.08 | 0.0013 | Significant |
| A-LOAD | 6.304E–06 | 1 | 6.304E–06 | 59.87 | 0.0006 | |
| B-SLIDING DISTANCE | 2.653E–06 | 1 | 2.653E–06 | 25.19 | 0.0040 | |
| C-DISK ROTATION | 3.042E–08 | 1 | 3.042E–08 | 0.2889 | 0.6140 | |
| Residual | 5.264E–07 | 5 | 1.053E–07 | | | |
| Cor Total | 0.0000 | 8 | | | | |

**Table 9.** ANOVA table for COF for As cast specimen.

| Source | Sum of squares | df | Mean square | *F*-value | *p*-value | |
|---|---|---|---|---|---|---|
| Model | 0.0035 | 3 | 0.0012 | 24.14 | 0.0021 | Significant |
| A-LOAD | 0.0018 | 1 | 0.0018 | 36.56 | 0.0018 | |
| B-SLIDING DISTANCE | 0.0011 | 1 | 0.0011 | 22.19 | 0.0053 | |
| C-DISK ROTATION | 0.0000 | 1 | 0.0000 | 0.7179 | 0.4355 | |
| Residual | 0.0002 | 5 | 0.0000 | | | |
| Cor Total | 0.0037 | 8 | | | | |

**Table 10.** Wear results for AR2T2 specimens.

| Run No. | Load (N) | Sliding distance (m) | Disk rotation (rpm) | SWR ($mm^3$/Nm) | COF |
|---|---|---|---|---|---|
| 1 | 10 | 500 | 200 | 0.00529 | 0.336 |
| 2 | 10 | 1500 | 400 | 0.00456 | 0.351 |
| 3 | 10 | 2500 | 600 | 0.00405 | 0.359 |
| 4 | 20 | 500 | 400 | 0.00461 | 0.348 |
| 5 | 20 | 1500 | 600 | 0.00425 | 0.354 |
| 6 | 20 | 2500 | 200 | 0.00315 | 0.363 |
| 7 | 30 | 500 | 200 | 0.00341 | 0.351 |
| 8 | 30 | 1500 | 400 | 0.00253 | 0.376 |
| 9 | 30 | 2500 | 600 | 0.00169 | 0.401 |

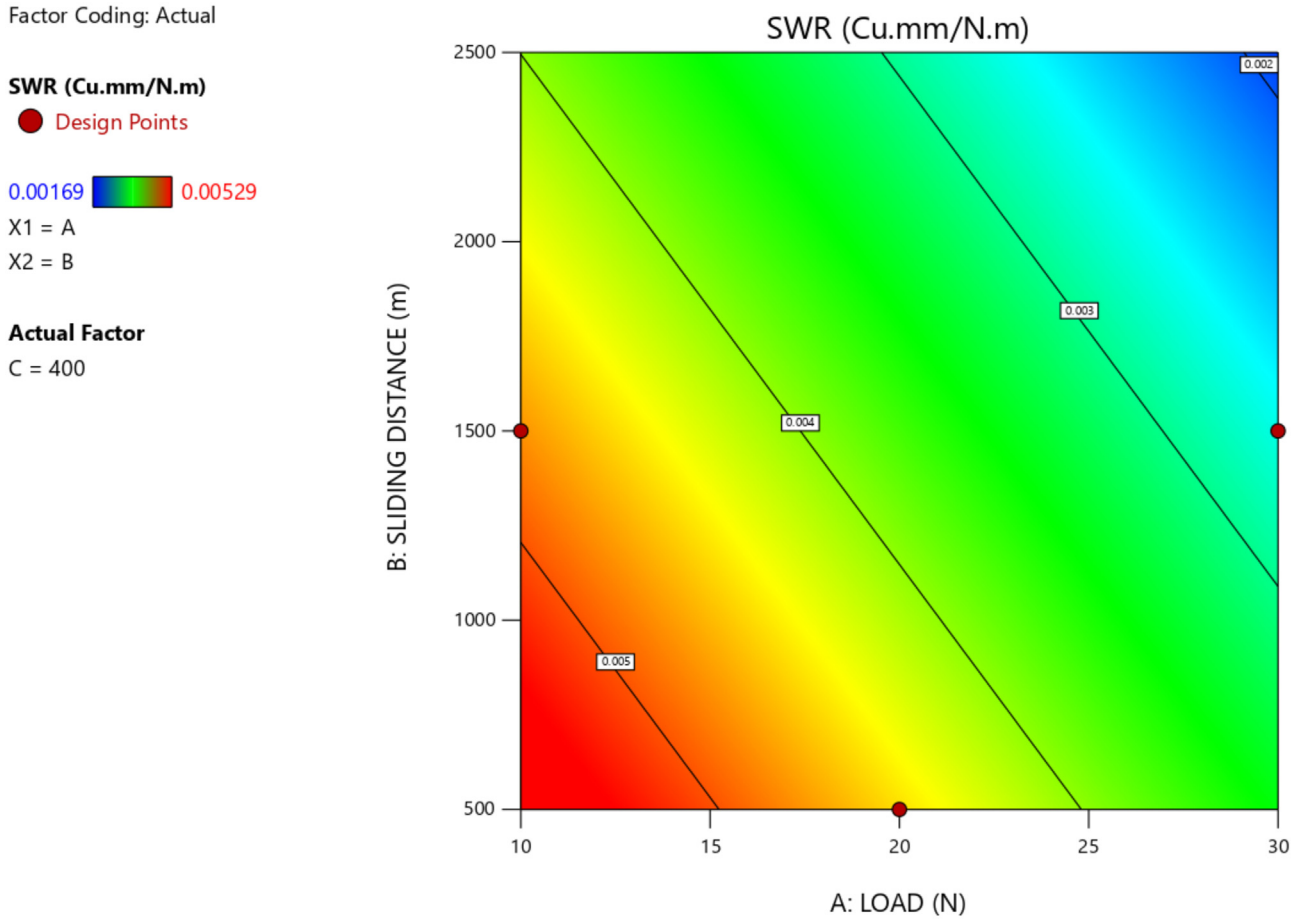


**Fig. 12.** Surface plot for variation of SWR with load and sliding distance for AR2T2 specimen.

### 3.2.1 Statistical validation of SWR for AR2T2 specimen

Figure 12 gives the surface plot, while Figure 13 gives the 3D contour plots for SWR for AR2T2 specimens. From, the surface and 3D contour plot, it is evident that the SWR reduces with the increment in the load and the sliding distance and it is much lesser than the As cast specimen.

Further, the regression correlation gives the fit data (Tab. 11) and the plot for curve fitting the predicted versus actual data (Fig. 14). While the equation (6) gives the regression equation from the RSM model for the SWR values obtained using the Design Expert Software. The increase in the COF increases the wear loss, however reduces the specific wear rate, due to the fact that the volumetric wear loss is relatively lesser as compared to the subsequent increase in the load and the sliding distance.

The predicted $R^2$ of 0.7446 is in reasonable agreement with the adjusted $R^2$ of 0.9264; i.e. the difference is less than 0.2.

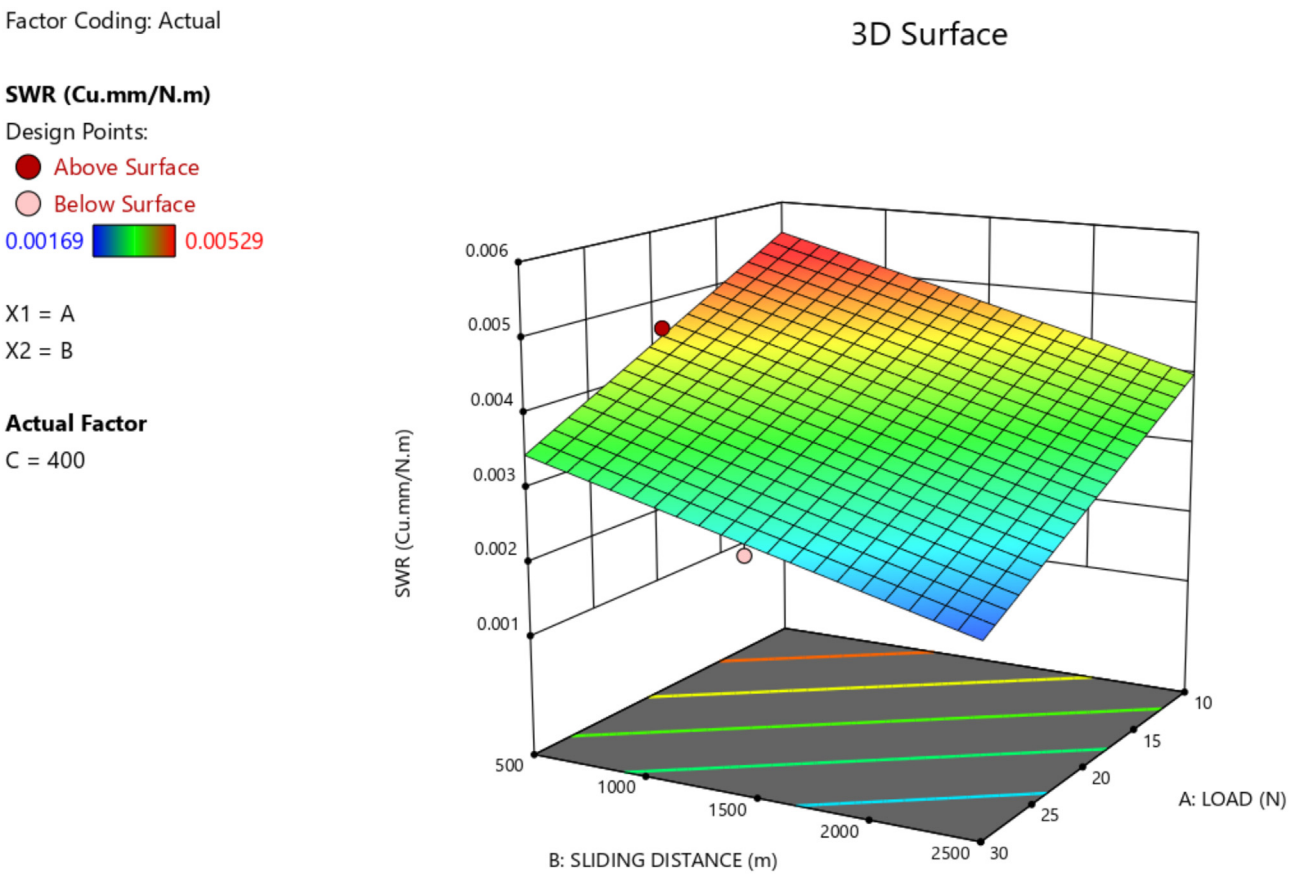


**Fig. 13.** 3D Contour plot for variation of SWR with load and sliding distance for AR2T2 specimen.

**Table 11.** Fit statistics of SWR for AR2T2 specimen.

| Std. Dev. | 0.0003 | $R^2$ | 0.9540 |
|---|---|---|---|
| Mean | 0.0037 | Adjusted $R^2$ | 0.9264 |
| C.V.% | 8.27 | Predicted $R^2$ | 0.7446 |
| | | Adeq Precision | 16.9708 |

Adeq Precision measures the signal to noise ratio. A ratio greater than 4 is desirable. The ratio of 16.971 indicates an adequate signal. This model can be used to navigate the design space.

$$\text{SWR} = +0.006824 - 0.000104 * \text{LOAD} - 7.756\text{E} - 7 * \text{SLIDING DISTANCE} + 3.889\text{E} - 7 * \text{DISK ROTATION}. \quad (6)$$

### 3.2.2 Statistical validation of COF for AR2T2 specimen

Figure 15 gives the surface plot, while Figure 16 gives the 3D contour plots for COF for AR2T2 specimens. From, the surface and 3D contour plot, it is evident that the COF increases with the increment in the load and the sliding distance and it is much lesser than the As cast specimen.

Further, the regression correlation gives the fit data (Tab. 12) and the plot for curve fitting the predicted vs. actual data (Fig. 17). While the equation (7) gives the regression equation from the RSM model for the COF values obtained using the Design Expert Software. The increase in the COF increases the wear loss, however reduces the Specific wear rate, due to the fact that the volumetric wear loss is relatively lesser as compared to the subsequent increase in the load and the sliding distance.

The predicted $R^2$ of 0.4416 is not as close to the adjusted $R^2$ of 0.7963 as one might normally expect; i.e. the difference is more than 0.2. This may indicate a large block effect. Things to consider are model reduction, response transformation, outliers, etc. All the empirical models are tested by doing confirmation runs.

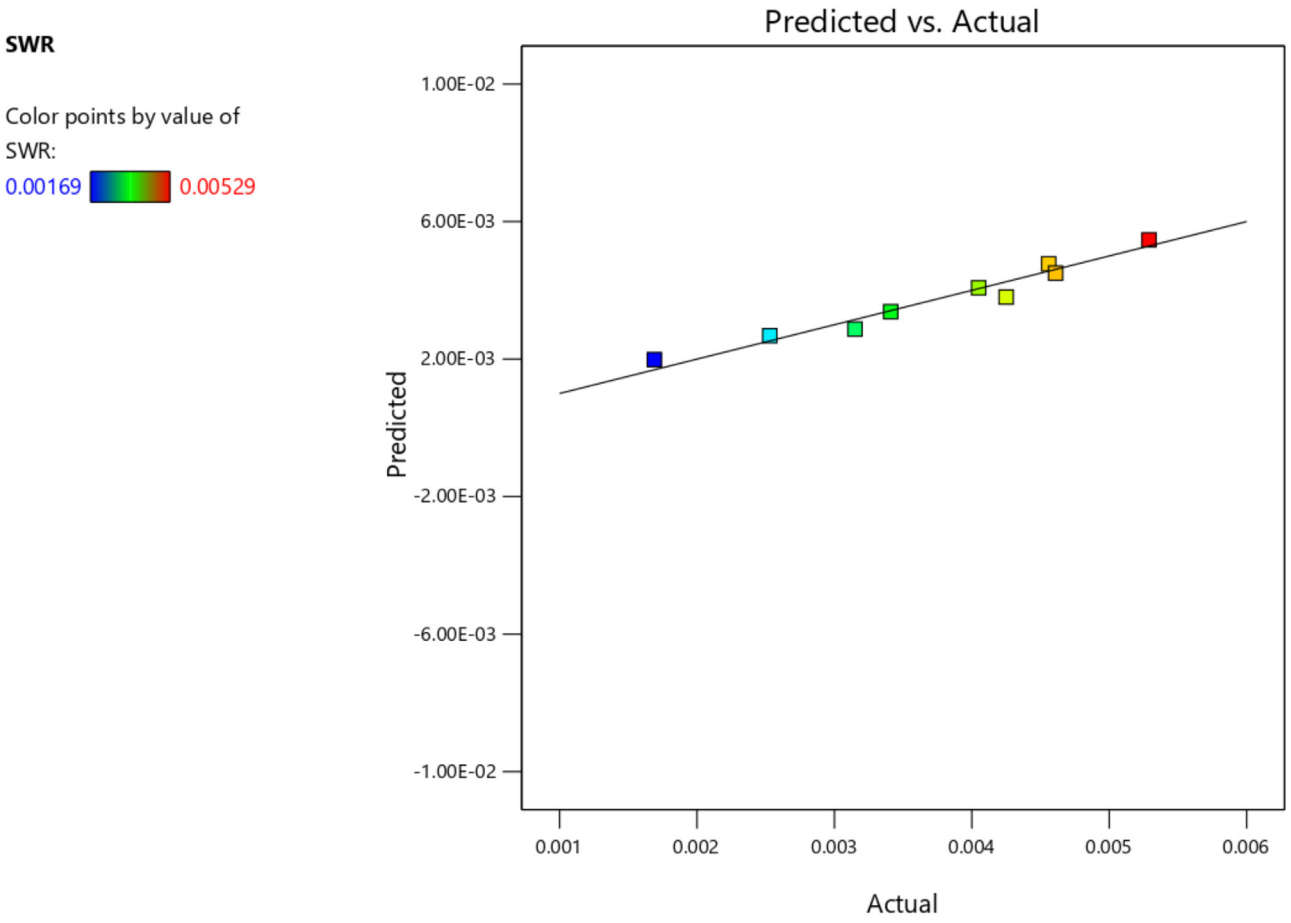


**Fig. 14.** Curve fitting for predicted versus actual values for SWR for AR2T2 specimen.

Adeq precision measures the signal to noise ratio. A ratio greater than 4 is desirable. The ratio of 10.734 indicates an adequate signal. This model can be used to navigate the design space.

$$\text{COF} = +0.305 + 0.001367 * \text{LOAD} + 0.000012 * \text{SLIDING DISTANCE} + 0.000022 * \text{DISK ROTATION}. \quad (7)$$

### 3.2.3 Analysis of variance (ANOVA) for AR2T2 specimen

Table 13 gives the ANOVA results for SWR for AR2T2 specimen. The model *F*-value of 34.54 implies the model is significant. There is only a 0.09% chance that an *F*-value this large could occur due to noise.

*P*-values less than 0.0500 indicate model terms are significant. In this case A, B are significant model terms. Values greater than 0.1000 indicate the model terms are not significant. If there are many insignificant model terms (not counting those required to support hierarchy), model reduction may improve the model.

Table 14 gives the ANOVA results for COF for AR2T2 specimen. The model *F*-value of 11.43 implies the model is significant. There is only a 1.12% chance that an *F*-value this large could occur due to noise.

*P*-values less than 0.0500 indicate model terms are significant. In this case A, B are significant model terms. Values greater than 0.1000 indicate the model terms are not significant. If there are many insignificant model terms (not counting those required to support hierarchy), model reduction may improve the model.

## 3.3 Effect of the different factors on COF and SWR for AR2T4 specimen

The effect of different set of factors on the COF and SWR are also evaluated for the AR2T4 specimen. The wear results are tabulated in Table 15.

### 3.3.1 Statistical validation of SWR for AR2T4 specimen

Figure 18 gives the surface plot, while Figure 19 gives the 3D contour plots for SWR for AR2T4 specimens. From, the surface and 3D contour plot, it is evident that the SWR reduces with the increment in the load and the sliding distance and it is much lesser than the As cast specimen.

Further, the regression correlation gives the fit data (Tab. 20) and the plot for curve fitting the predicted versus actual data (Fig. 20). While the equation (8) gives the regression equation from the RSM model for the SWR values obtained using the Design Expert Software.

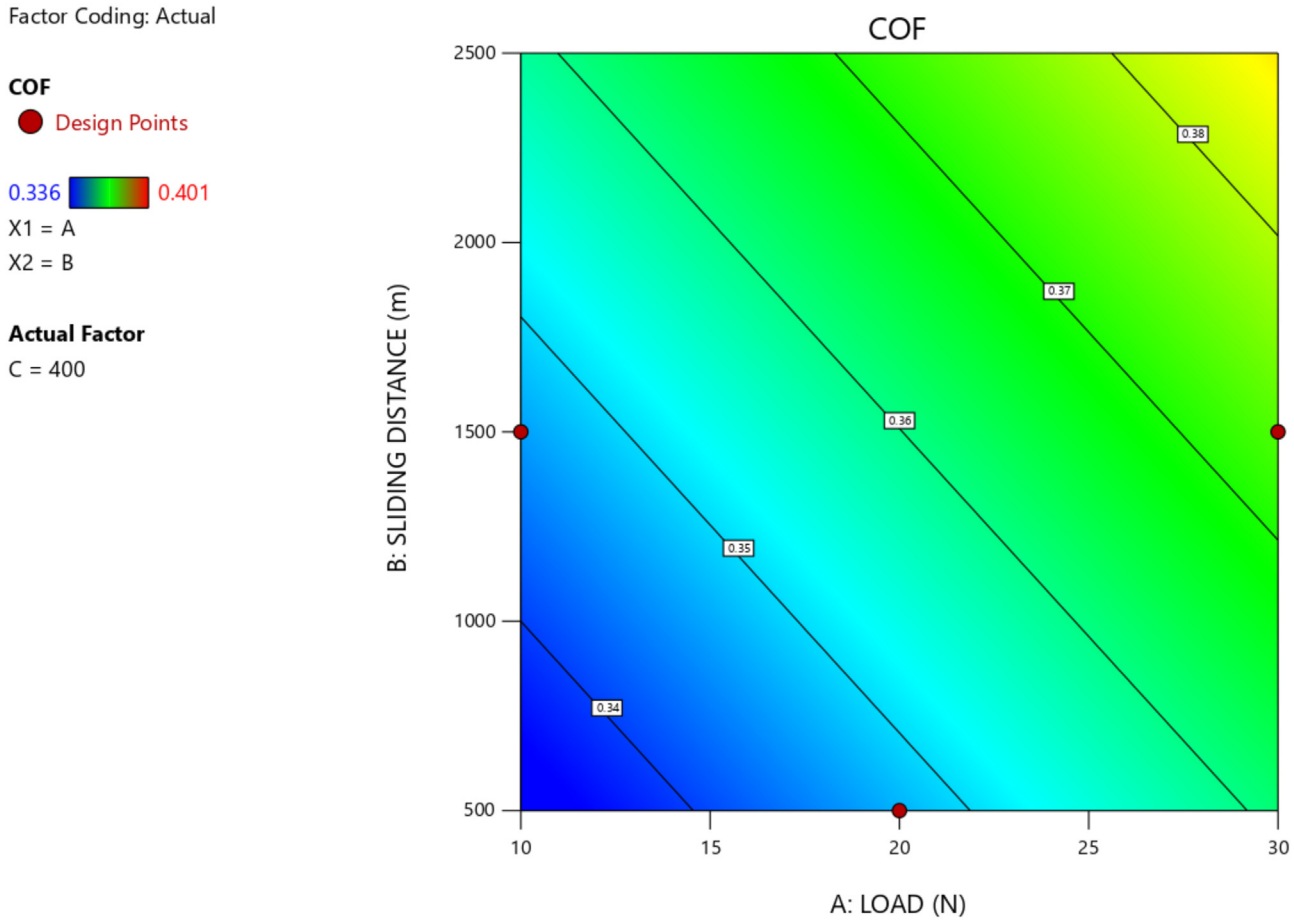


**Fig. 15.** Surface plot for variation of COF with load and sliding distance for AR2T2.

The predicted $R^2$ of 0.7401 is in reasonable agreement with the adjusted $R^2$ of 0.9241; i.e. the difference is less than 0.2.

Adeq precision measures the signal to noise ratio. A ratio greater than 4 is desirable. The ratio of 16.612 indicates an adequate signal. This model can be used to navigate the design space.

$$\begin{aligned}\text{SWR} = {} & +0.006253 - 0.000101 * \text{LOAD} - 7.667\text{E} - 7 \\ & * \text{SLIDING DISTANCE} + 4.833\text{E} - 7 \\ & * \text{DISK ROTATION}. \end{aligned} \tag{8}$$

### 3.3.2 Statistical validation of COF for AR2T4 specimen

Figure 21 gives the surface plot, while Figure 22 gives the 3D contour plots for COF for AR2T4 specimens. From, the surface and 3D contour plot, it is evident that the COF increases with the increment in the load and the sliding distance.

Further, the regression correlation gives the fit data (Tab. 17) and the plot for curve fitting the predicted versus actual data (Fig. 23). While the equation (9) gives the regression equation from the RSM model for the COF values obtained using the Design Expert Software. The COF for AR2T4 specimen is relative lesser than that of the AR2T2 specimen.

The predicted $R^2$ of 0.7805 is in reasonable agreement with the adjusted $R^2$ of 0.9064; i.e. the difference is less than 0.2.

Adeq precision measures the signal to noise ratio. A ratio greater than 4 is desirable. The ratio of 16.533 indicates an adequate signal. This model can be used to navigate the design space.

$$\begin{aligned}\text{SWR} = {} & +0.301 + 0.0013 * \text{LOAD} + 0.000012 \\ & * \text{SLIDING DISTANCE} + 0.000025 \\ & * \text{DISK ROTATION}. \end{aligned} \tag{9}$$

### 3.3.3 ANOVA for AR2T4 specimen

Table 18 gives the ANOVA table for SWR for AR2T4 specimen. The model $F$-value of 33.45 implies the model is significant. There is only a 0.10% chance that an $F$-value this large could occur due to noise.

$P$-values less than 0.0500 indicate model terms are significant. In this case A, B are significant model terms. Values greater than 0.1000 indicate the model terms are not significant. If there are many insignificant model terms (not counting those required to support hierarchy), model reduction may improve the model.

Table 19 gives the ANOVA table for COF for AR2T4 specimen. The model $F$-value of 26.81 implies the model is significant. There is only a 0.17% chance that an $F$-value this large could occur due to noise.

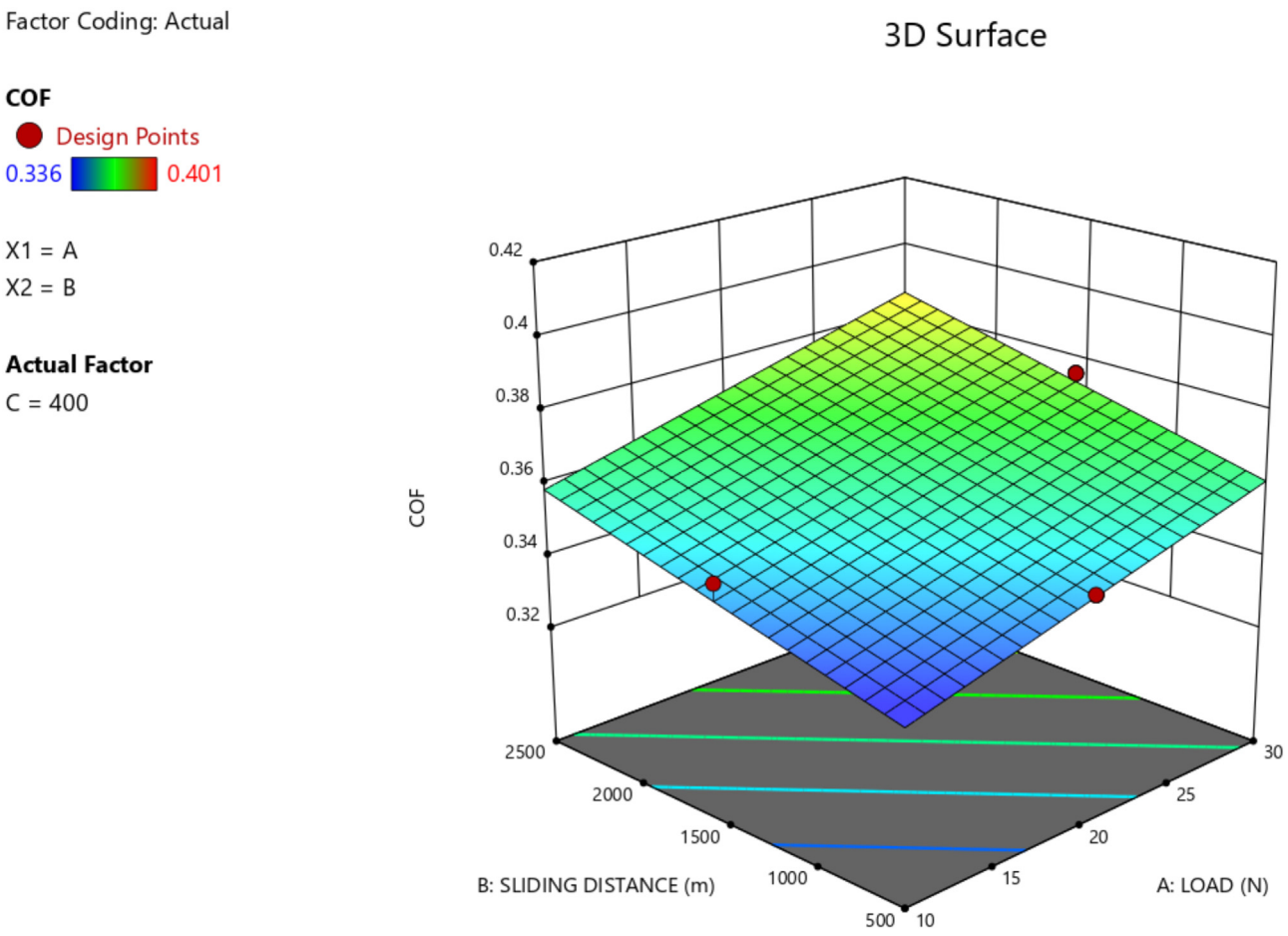


**Fig. 16.** 3D contour plot for variation of COF with load and sliding distance for AR2T2.

**Table 12.** Fit statistics of COF for AR2T2 specimen.

| Std. Dev. | 0.0085 | $R^2$ | 0.8727 |
|---|---|---|---|
| Mean | 0.3599 | Adjusted $R^2$ | 0.7963 |
| C.V.% | 2.37 | Predicted $R^2$ | 0.4416 |
| | | Adeq Precision | 10.7337 |

*P*-values less than 0.0500 indicate model terms are significant. In this case A, B are significant model terms. Values greater than 0.1000 indicate the model terms are not significant. If there are many insignificant model terms (not counting those required to support hierarchy), model reduction may improve the model.

## 3.4 Effect of the different factors on COF and SWR for AR2T6 specimen

The effect of different set of factors on the COF and SWR are also evaluated for the AR2T4 specimen. The wear results are tabulated in Table 20.

### 3.4.1 Statistical validation of SWR for AR2T6 specimen

Figure 24 gives the surface plot, while Figure 25 gives the 3D contour plots for SWR for AR2T6 specimens. From, the surface and 3D contour plot, it is evident that the SWR reduces with the increment in the load and the sliding distance.

Further, the regression correlation gives the fit data (Tab. 20) and the plot for curve fitting the predicted versus actual data (Fig. 26). While the equation (10) gives the regression equation from the RSM model for the SWR values obtained using the Design Expert Software. The SWR for AR2T6 specimen increases as compared to the AR2T4 specimen.

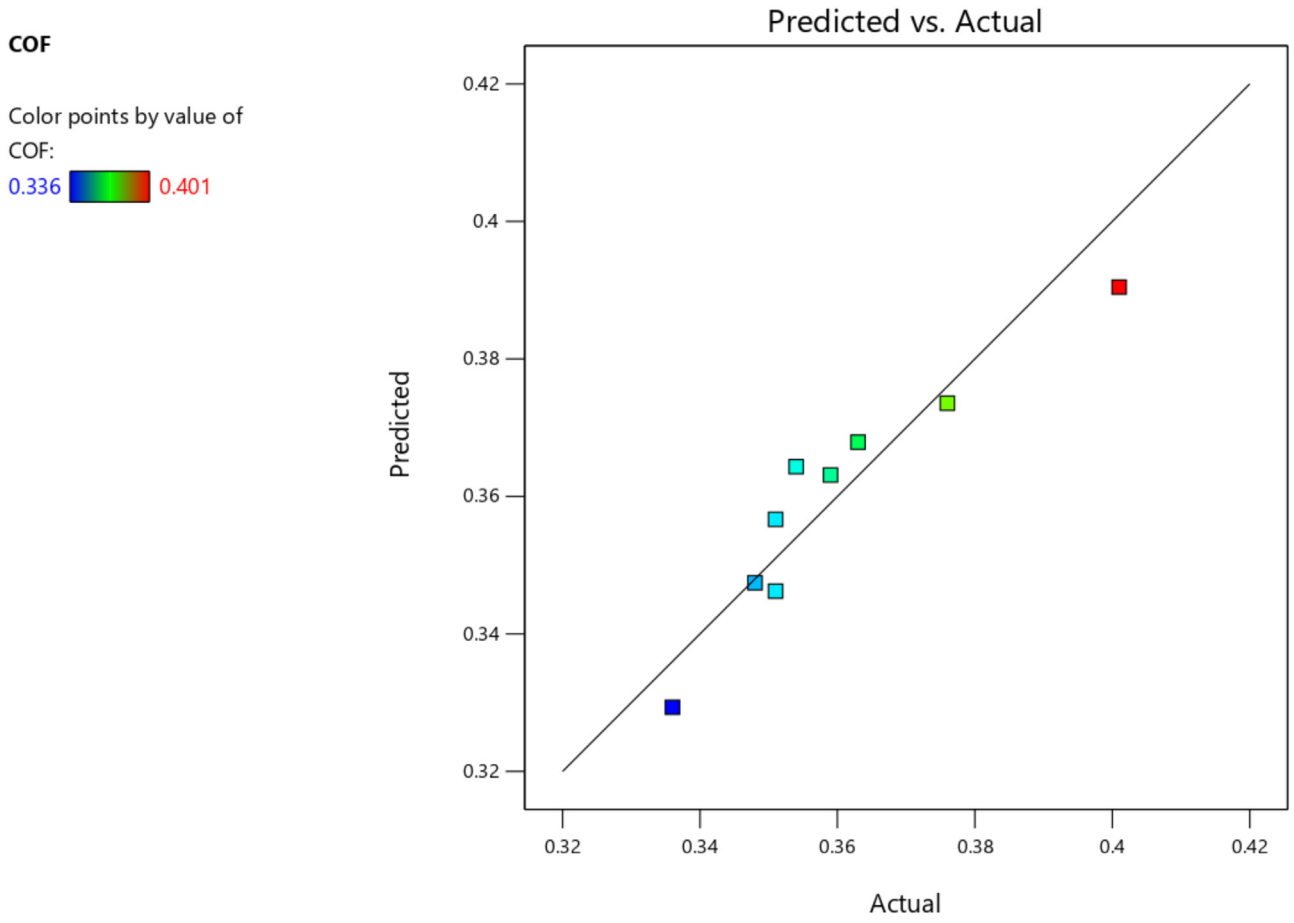


**Fig. 17.** Curve fitting for predicted versus actual values for COF for AR2T2.

**Table 13.** ANOVA table for SWR for AR2T2 specimen.

| Source | Sum of squares | df | Mean Square | *F*-value | *p*-value | Remarks |
|---|---|---|---|---|---|---|
| Model | 9.835E-06 | 3 | 3.278E-06 | 34.54 | 0.0009 | Significant |
| A-LOAD | 6.552E-06 | 1 | 6.552E-06 | 69.03 | 0.0004 | |
| B-SLIDING DISTANCE | 2.707E-06 | 1 | 2.707E-06 | 28.52 | 0.0031 | |
| C-DISK ROTATION | 2.722E-08 | 1 | 2.722E-08 | 0.2868 | 0.6152 | |
| Residual | 4.746E-07 | 5 | 9.491E-08 | | | |
| Cor Total | 0.0000 | 8 | | | | |

**Table 14.** ANOVA table for COF for AR2T2 specimen.

| Source | Sum of squares | df | Mean square | *F*-value | *p*-value | Remarks |
|---|---|---|---|---|---|---|
| Model | 0.0025 | 3 | 0.0008 | 11.43 | 0.0112 | Significant |
| A-LOAD | 0.0011 | 1 | 0.0011 | 15.37 | 0.0112 | |
| B-SLIDING DISTANCE | 0.0007 | 1 | 0.0007 | 9.26 | 0.0271 | |
| C-DISK ROTATION | 0.0001 | 1 | 0.0001 | 1.22 | 0.3199 | |
| Residual | 0.0004 | 5 | 0.0001 | | | |
| Cor Total | 0.0029 | 8 | | | | |

**Table 15.** SWR for COF and AR2T4 specimen.

| AR2T4 Specimen | | | | | |
|---|---|---|---|---|---|
| Run No. | Load (N) | Sliding distance (m) | Disk rotation (rpm) | SWR ($mm^3/Nm$) | COF |
| 1 | 10 | 500 | 200 | 0.00471 | 0.328 |
| 2 | 10 | 1500 | 400 | 0.00411 | 0.341 |
| 3 | 10 | 2500 | 600 | 0.00359 | 0.354 |
| 4 | 20 | 500 | 400 | 0.00416 | 0.349 |
| 5 | 20 | 1500 | 600 | 0.00376 | 0.357 |
| 6 | 20 | 2500 | 200 | 0.00265 | 0.363 |
| 7 | 30 | 500 | 200 | 0.00302 | 0.344 |
| 8 | 30 | 1500 | 400 | 0.00204 | 0.368 |
| 9 | 30 | 2500 | 600 | 0.00128 | 0.389 |

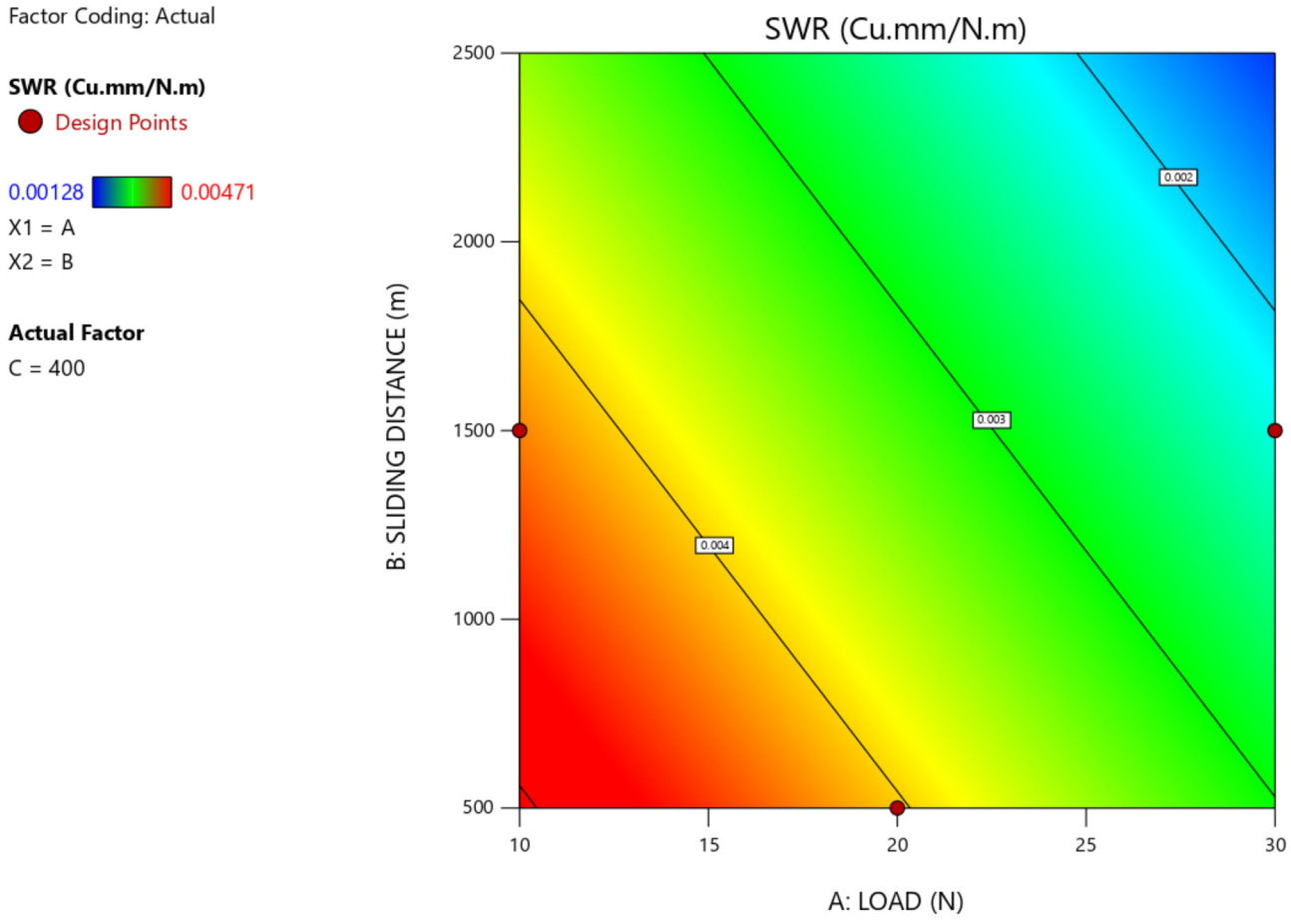


**Fig. 18.** Surface plot for variation of SWR with load and sliding distance for AR2T4 specimen.

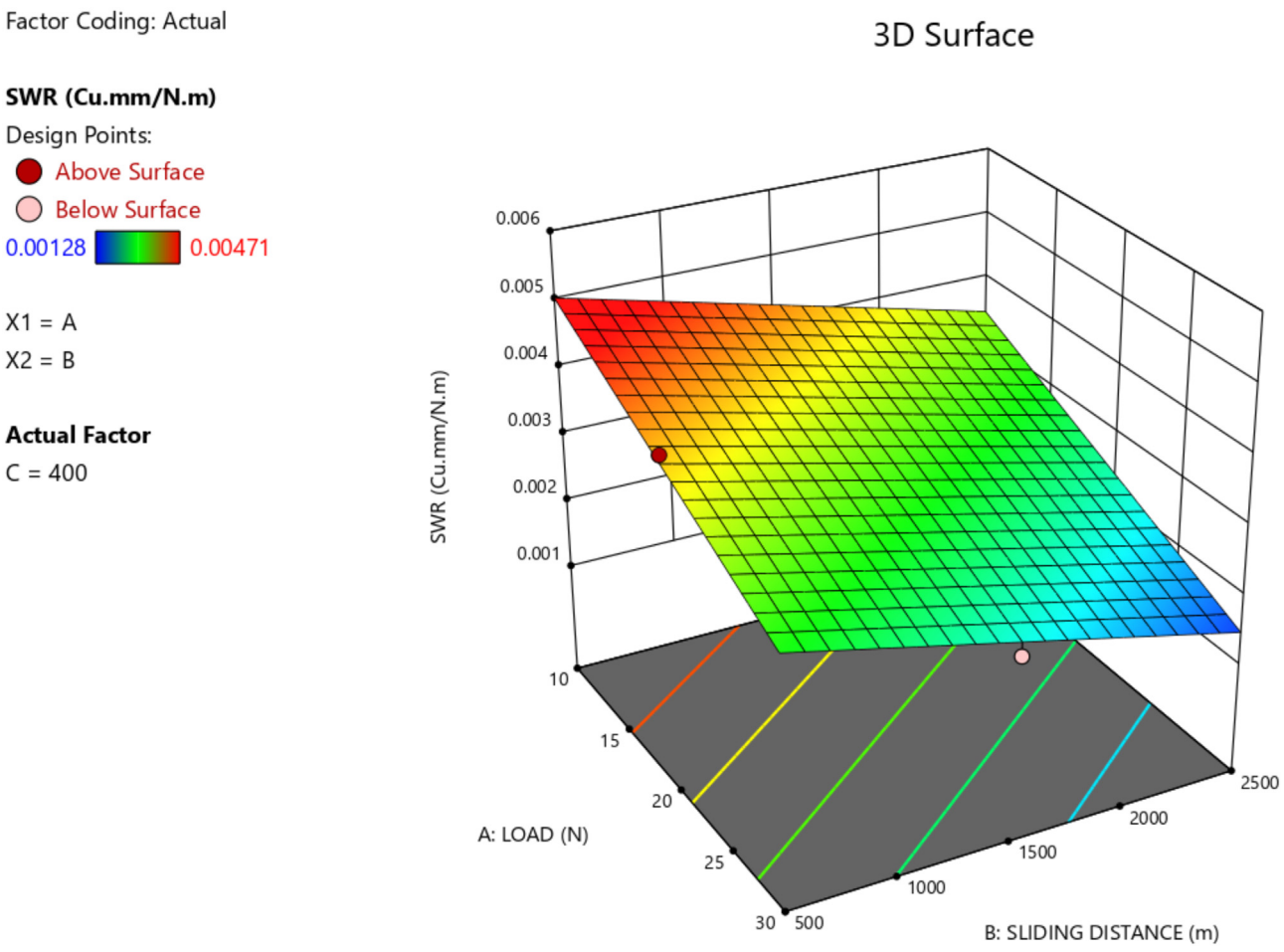


**Fig. 19.** 3D Contour plot for variation of SWR with load and sliding distance for AR2T4 specimen.

**Table 16.** Fit statistics of wear test for As cast specimen.

| Std. Dev. | 0.0003 | $R^2$ | 0.9525 |
|---|---|---|---|
| Mean | 0.0033 | Adjusted $R^2$ | 0.9241 |
| C.V.% | 9.38 | Predicted $R^2$ | 0.7401 |
| | | Adeq precision | 16.6117 |

**Table 17.** Fit statistics of wear test for As cast specimen.

| Std. Dev. | 0.0054 | $R^2$ | 0.9415 |
|---|---|---|---|
| Mean | 0.3548 | Adjusted $R^2$ | 0.9064 |
| C.V.% | 1.52 | Predicted $R^2$ | 0.7805 |
| | | Adeq precision | 16.5332 |

**Table 18.** ANOVA for SWR for AR2T4.

| Source | Sum of squares | df | Mean square | *F*-value | *p*-value | Remarks |
|---|---|---|---|---|---|---|
| Model | 9.366E-06 | 3 | 3.122E-06 | 33.45 | 0.0010 | Significant |
| A-LOAD | 6.141E-06 | 1 | 6.141E-06 | 65.79 | 0.0005 | |
| B-SLIDING DISTANCE | 2.714E-06 | 1 | 2.714E-06 | 29.08 | 0.0030 | |
| C-DISK ROTATION | 4.205E-08 | 1 | 4.205E-08 | 0.4505 | 0.5318 | |
| Residual | 4.667E-07 | 5 | 9.333E-08 | | | |
| Cor Total | 9.832E-06 | 8 | | | | |

**Table 19.** ANOVA for COF for AR2T4.

| Source | Sum of squares | df | Mean square | *F*-value | *p*-value | Remarks |
|---|---|---|---|---|---|---|
| Model | 0.0023 | 3 | 0.0008 | 26.81 | 0.0017 | Significant |
| A-LOAD | 0.0010 | 1 | 0.0010 | 34.99 | 0.0020 | |
| B-SLIDING DISTANCE | 0.0006 | 1 | 0.0006 | 21.14 | 0.0059 | |
| C-DISK ROTATION | 0.0001 | 1 | 0.0001 | 3.88 | 0.1059 | |
| Residual | 0.0001 | 5 | 0.0000 | | | |
| Cor Total | 0.0025 | 8 | | | | |

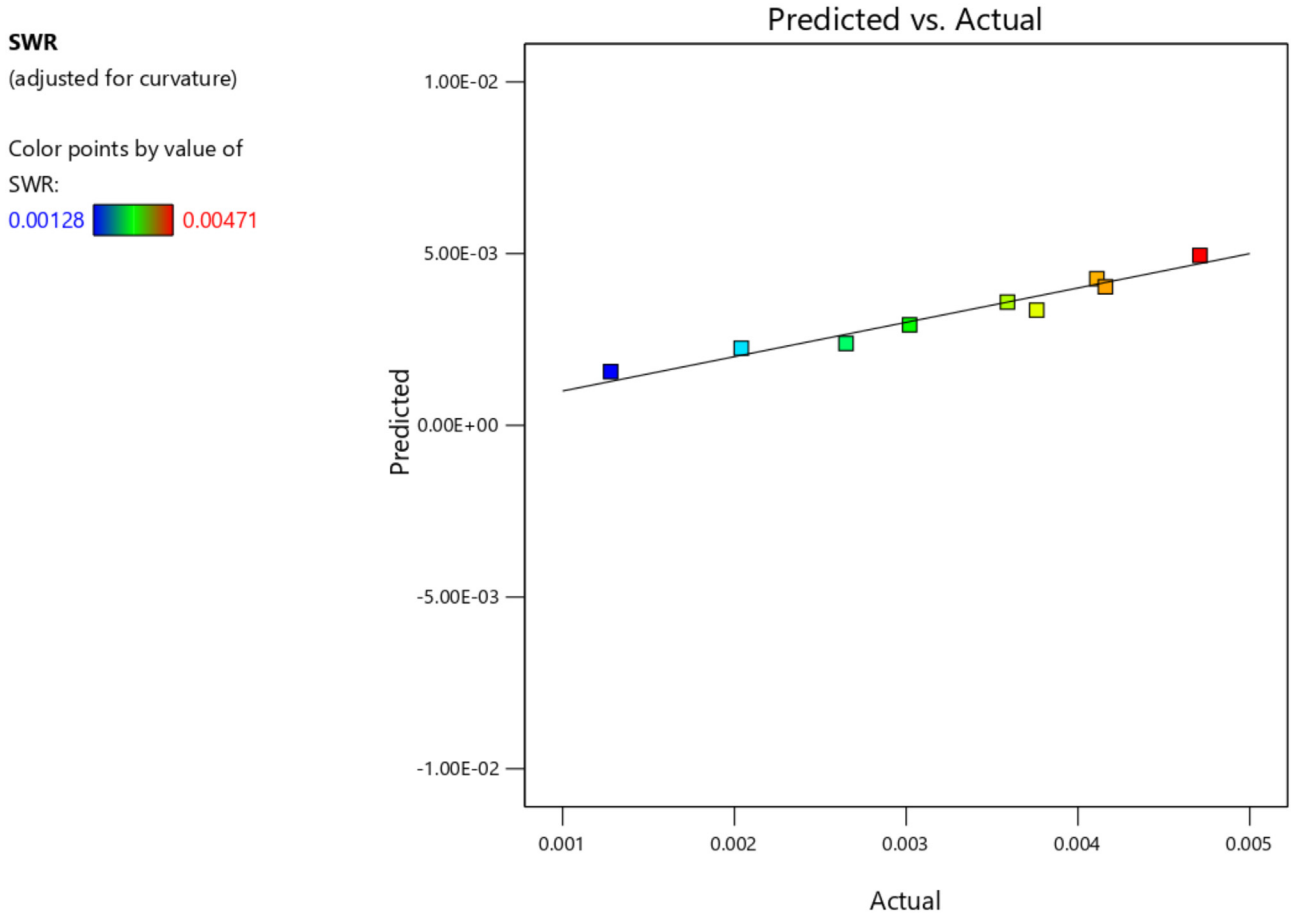


**Fig. 20.** Curve fitting for predicted versus actual values for SWR for AR2T4 specimen.

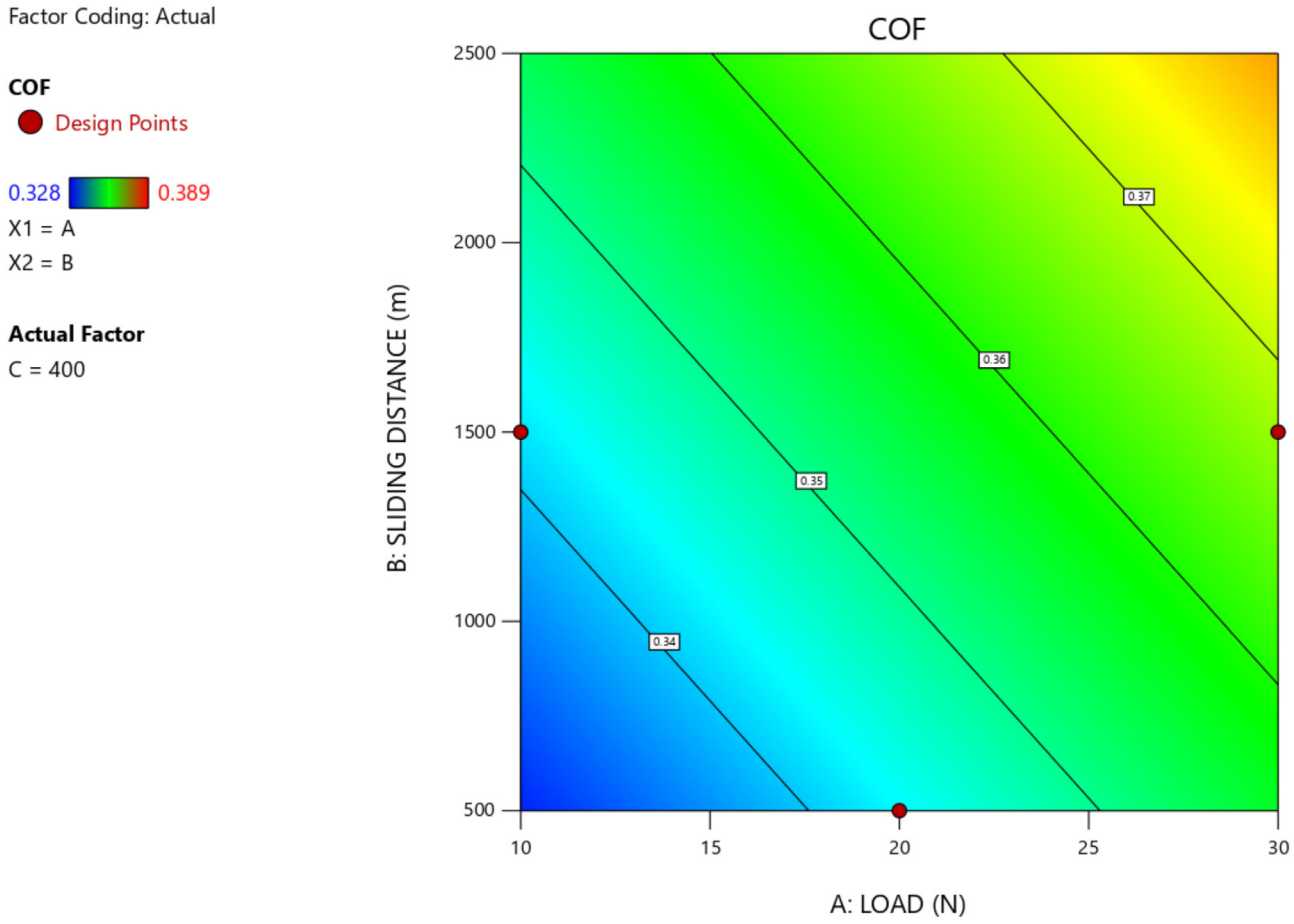


**Fig. 21.** Surface plot for variation of COF with load and sliding distance for AR2T4 specimen.

The predicted $R^2$ of 0.9654 is in reasonable agreement with the adjusted $R^2$ of 0.9803; i.e. the difference is less than 0.2.

Adeq Precision measures the signal to noise ratio. A ratio greater than 4 is desirable. The ratio of 36.101 indicates an adequate signal. This model can be used to navigate the design space.

$$\begin{aligned}\text{SWR} = {} & +0.005969 - 0.000046 * \text{LOAD} - 4.744\text{E} - 7 \\ & * \text{SLIDING DISTANCE} - 5.056\text{E} - 7 \\ & * \text{DISK ROTATION}. \end{aligned} \quad (10)$$

### 3.4.2 Statistical validation of COF for AR2T6 specimen

Figure 27 gives the surface plot, while Figure 28 gives the 3D contour plots for COF for AR2T6 specimens and Figure 29 Curve fitting for predicted versus actual values for COF for AR2T6 specimens From, the surface and 3D contour plot, it is evident that the COF increases with the increment in the load and the sliding distance.

Further, the regression correlation gives the fit data (Tab. 21) and the plot for curve fitting the predicted versus actual data (Fig. 26). While the equation (11) gives the regression equation from the RSM model for the COF values obtained using the Design Expert Software. The COF values of AR2T6 specimen increases with the increase in the weight percentage of $TiO_2$ due to the ridges and valleys that are formed by the agglomeration of the reinforcements beyond 4 wt.% of $TiO_2$ in some localized regions and presence of voids in other regions attributed to inhomogeneous distribution. This agglomeration of the ceramic compounds in the form of oxides increase the coefficient of friction between the rubbing surfaces in wear test. The increase in the wear tracks for AR2T6 spcimen is also evident in the SEM images in Figure 31. This is also ascertained from the findings of Santhosh et al. [37,38], and Bharath et al. [39], who have reported the influence of reinforcements on the wear and hardness characteristics of the composite materials. The presence of ceramic compounds beyond a certain limit are found to cause embrittlement in certain regions and pores in other regions due to microcoring and segregation.

The predicted $R^2$ of 0.5604 is not as close to the adjusted $R^2$ of 0.8867 as one might normally expect; i.e. the difference is more than 0.2. This may indicate a large block effect or a possible problem with the model and/or data. Things to consider are model reduction, response transformation, outliers, etc. All empirical models should be tested by doing confirmation runs.

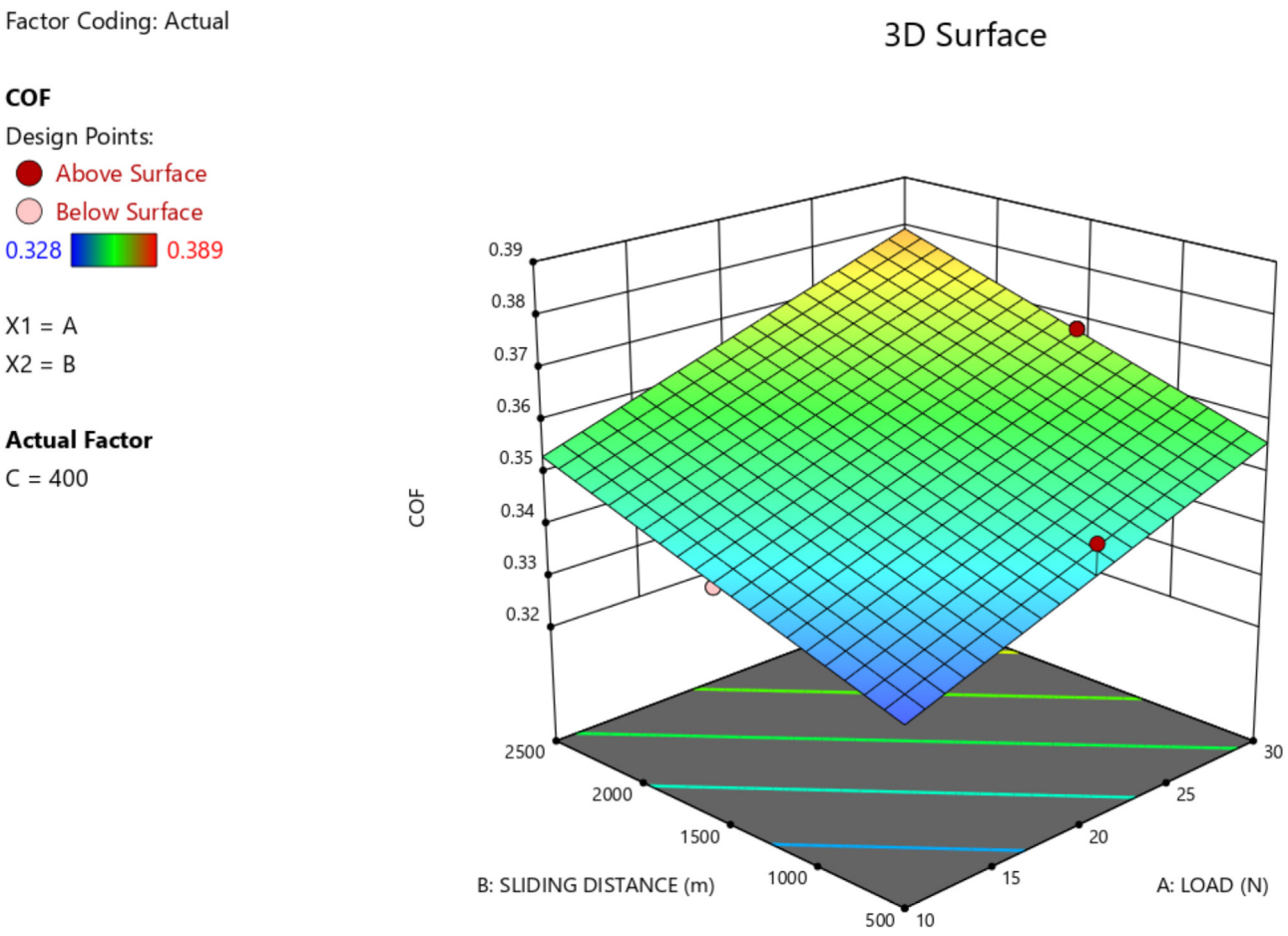


**Fig. 22.** 3D contour plot for variation of COF with load and sliding distance for AR2T4 specimen.

Adeq precision measures the signal to noise ratio. A ratio greater than 4 is desirable. The ratio of 14.337 indicates an adequate signal. This model can be used to navigate the design space.

$$\begin{aligned}\mathrm{COF} = {} & +0.322944 + 0.001567 * \mathrm{LOAD} + 9\mathrm{E} - 6 \\ & * \mathrm{SLIDINGDISTANCE} + 0.000013 \\ & * \mathrm{DISKROTATION}. \end{aligned} \quad (11)$$

### 3.4.3 ANOVA for AR2T6

Table 22 gives the ANOVA for SWR for AR2T6 specimens. The model $F$-value of 133.62 implies the model is significant. There is only a 0.01% chance that an $F$-value this large could occur due to noise.

$P$-values less than 0.0500 indicate model terms are significant. In this case A, B are significant model terms. Values greater than 0.1000 indicate the model terms are not significant. If there are many insignificant model terms (not counting those required to support hierarchy), model reduction may improve the model.

Table 23 gives the ANOVA for COF for AR2T6 specimens. The model $F$-value of 21.86 implies the model is significant. There is only a 0.27% chance that an $F$-value this large could occur due to noise.

$P$-values less than 0.0500 indicate model terms are significant. In this case A, B are significant model terms. Values greater than 0.1000 indicate the model terms are not significant. If there are many insignificant model terms (not counting those required to support hierarchy), model reduction may improve the model.

## 3.5 Comparisons for SWR and COF for different composite specimens

The comparative evaluation of the SWR and COF values for different composite specimens as shown in Figures 30–31 clearly depicts that the SWR reduces with the inclusion of the red mud and $TiO_2$ reinforcements in the matrix. This is due to the embrittlement and subsequent increase in the hardness caused by the ceramic compounds viz., the oxides of Ti, and the oxides of Al, Fe in the redmud. However, the increase in the $TiO_2$ content beyond 4 wt.% increases the SWR and COF owing to the agglomeration of the reinforcements at certain localized regions and formation of the voids at other locations resulting in reduced hardness of the composites. Henceforth, it is evident that the optimum wt.% of reinforcements for improving the wear characteristics in the composites is 2 wt.% red mud and 4 wt.% $TiO_2$, beyond which the wear resistance of the composites reduces.

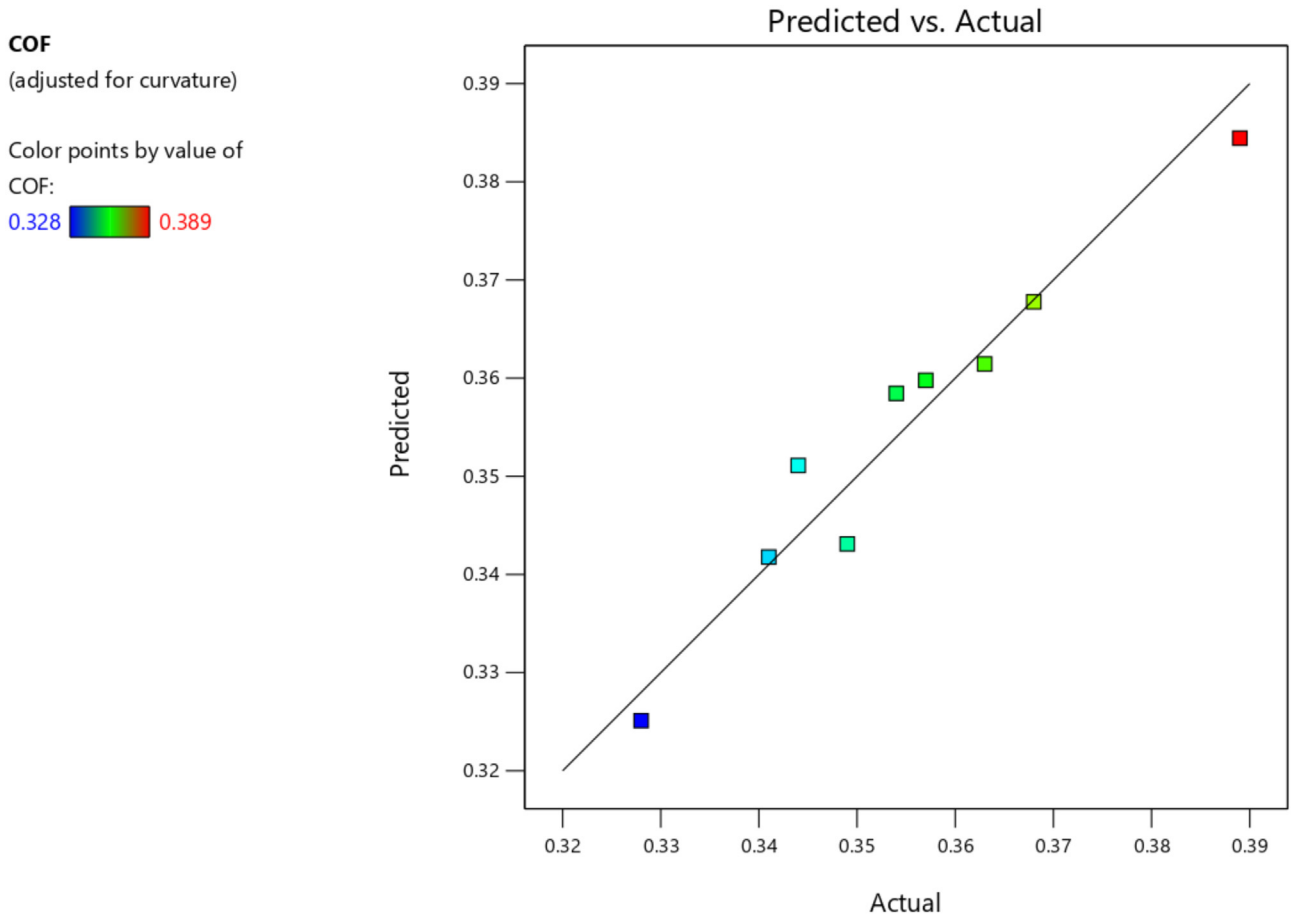


**Fig. 23.** Curve fitting for predicted versus actual values for COF for AR2T4 specimen.

### 3.6 Coefficient of friction (COF) with time for different composition

The variation of the coefficient of friction with time for different composition give an idea of the variation of the friction forces during the test period. It helps to identify the wear profile for different composite specimens for which the tribological tests are accomplished. The COF for as cast specimen is found to be maximum in comparison with the other composites. However, as the reinforcements are included in the composites, the coefficient of friction decreases upto 4 wt.% of $TiO_2$, beyond which the COF slightly increases owing to microcoring and aggregations. Figures 32–35 give the curves of coefficient of friction (COF) variation with test time for 'As Cast', 'AR2T2', 'AR2T4', and 'AR2T6' specimen. The curves of COF variation with test time gives an understanding of the friction profile for the composite specimens.

The COF variation is predominant for the AR2T4 specimens, with significantly lesser COF in comparison with the "As Cast" and other composite specimens. This is due to stronger bonding between the matrix and reinforcements. The COF for As Cast specimen is higher than the average value and it reduces with the inclusion of red mud and $TiO_2$ inoculants in the matrix. However, for the AR2T6 specimen, the COF once again increases justifying the increase in the wear rate due to the existence of agglomerated zones in certain locations and voids in other regions.

### 3.7 Scanning electron microscopy of wear track

The SEM of the wear track of the composite specimens for wt.% of the reinforcements are depicted in Figure 36. It is evident from the SEM images that more number of ridges and valleys are seen in the as cast specimen, while the number of ridges, valleys and the wear tracks reduces with the increment in the wt.% of the reinforcements. The reduction in the number of wear tracks is attributed to the formation of friction films that resist the indentation and surface abrasion.

Figure 36a gives the SEM image of the As cast specimen with damaged surfaces and distinct ridges and valleys. While, Figure 36b gives the SEM image of the AR2T2 specimen with wear debris and thin layers of friction films, which begin to form with the inclusion of the reifnorcements. Figure 36c gives the SEM image of the AR2T4 specimen with thick friction films that resist the wear and tear of the specimens. Figure 3d gives the SEM image of the AR2T6 specimen, wherein the wear tracks again appear due to the exposure of softer layers of the surface to the wear and indentation, attributed majorly due to the agglomeration of reinforcements at certain localized regions, and formation of voids at other regions.

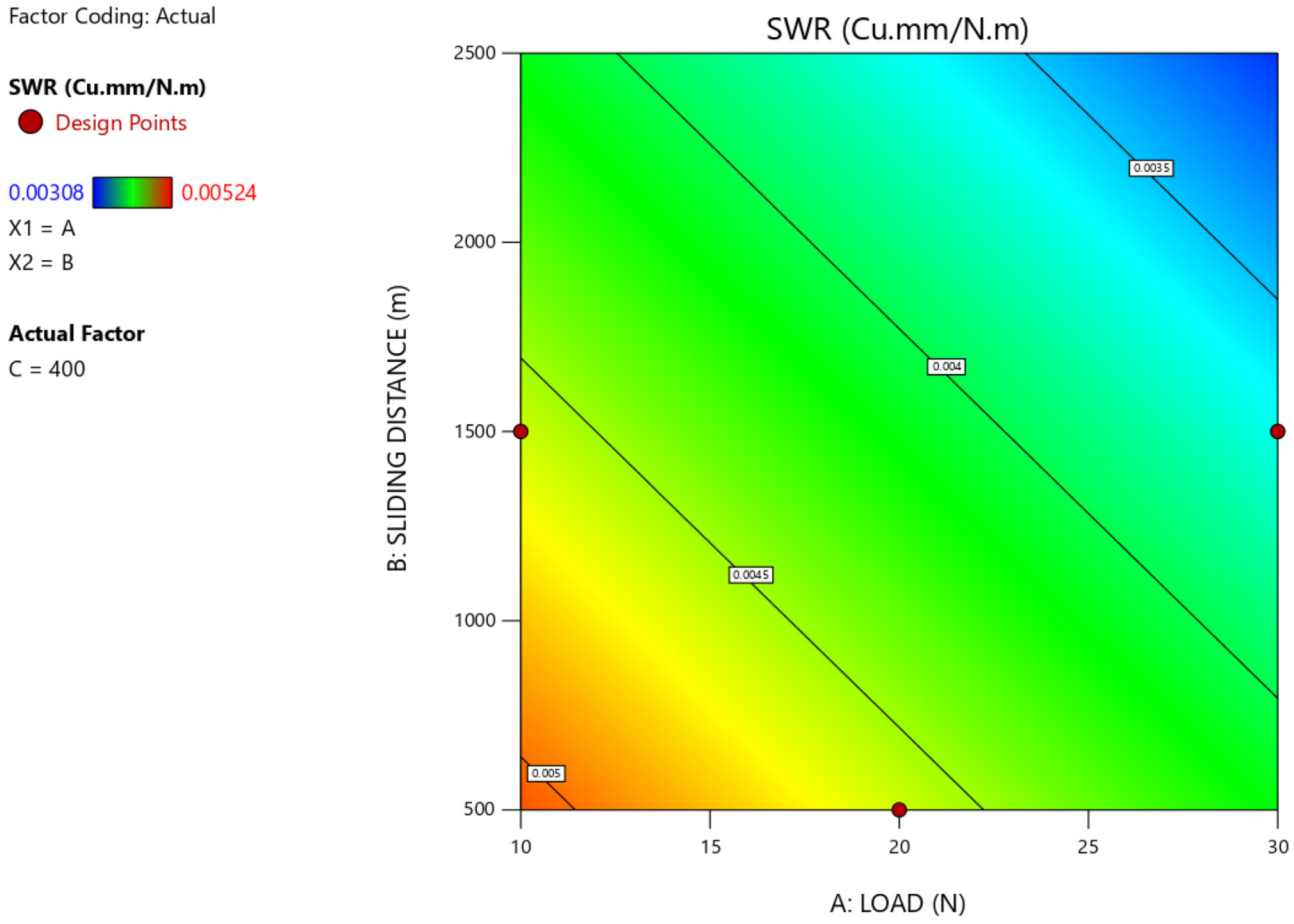


**Fig. 24.** Surface plot for variation of SWR with load and sliding distance for AR2T6 specimen.

## 4 Conclusions

The aluminium AA 6061-$TiO_2$-redmud composites fabricated are characterized for the wear. It is evident from the experimental observations and the statistical validations that the specific wear rate (SWR) and the coefficient of friction (COF) reduce with the inclusion of reinforcements, especially the red mud and $TiO_2$. However, the addition of red mud and $TiO_2$ beyond certain limit leads to agglomeration at certain localized regions and void formations at other regions.

The statistical analysis of the wear results also ascertains the experimental findings and the predicted results are in close agreement with the experimental values. The error between the experimental output and the predicted values are within ±10% band.

The SWR is maximum (0.00626 $mm^3/m$) for as cast specimen for R1 experimental trial (load of 10 N, sliding distance of 500 m, disk rotation speed of 200 rpm, while the SWR is minimum (0.00128 $mm^3/m$) for AR2T4 composite specimen with 2 wt.% red mud and 4 wt.% $TiO_2$ for R9 experimental trial (load of 30 N, sliding distance of 2500 m, and disk rotation speed of 600 rpm).

The COF is maximum for As Cast composite specimen (0.411) for R9 experimental trial viz., load of 30 N, sliding distance of 2500 m, disk rotation speed of 600 rpm, while the COF is minimum for AR2T4 composite specimen for R1 experimental trial viz., the load of 10 N, sliding distance of 500 m, disk rotation speed of 200 rpm.

Further, the SEM images also depict the formation of thick friction films with the inclusion of the red mud and $TiO_2$ reinforcements, leading to a decrease in the wear rate of the composite specimens. However, an increase in the $TiO_2$ content beyond 4 wt.% leads to localized agglomeration and void formations resulting in distinct pattens of wear in the composite specimens.

Henceforth, from the findings of the the present work, it is evident that the inclusion of the hybrid combination of red mud and $TiO_2$ reinforcements upto a certain threshold limit improves the triblogical characteristics of the composites.

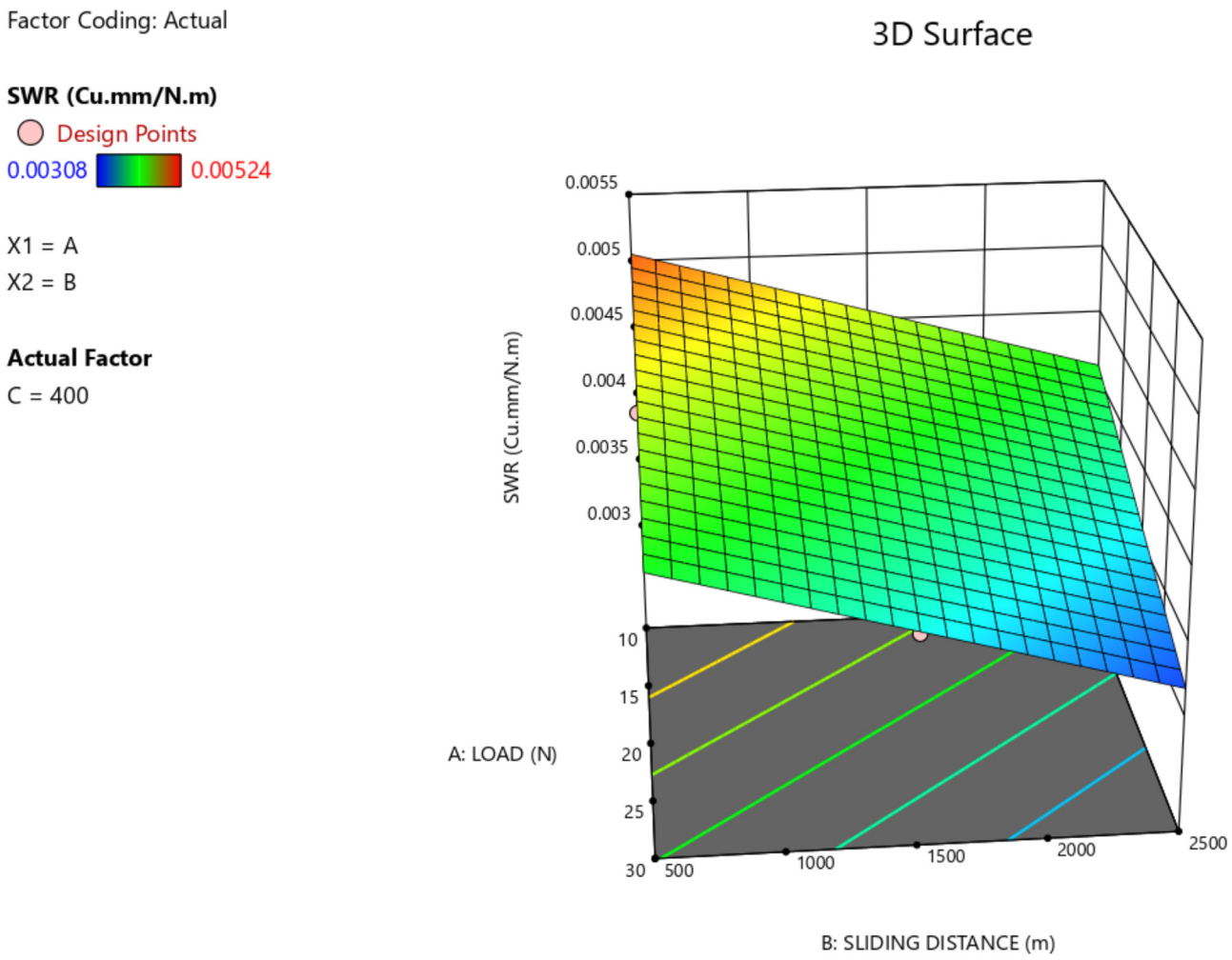


**Fig. 25.** 3D Contour plot for variation of SWR with load and sliding distance for AR2T6 specimen.

**Table 20.** Fit Statistics of wear test for As cast specimen.

| AR2T6 | | | | | |
|---|---|---|---|---|---|
| Run No. | Load (N) | Sliding distance (m) | Disk rotation (rpm) | SWR ($mm^3$/Nm) | COF |
| 1 | 10 | 500 | 200 | 0.00524 | 0.341 |
| 2 | 10 | 1500 | 400 | 0.00452 | 0.355 |
| 3 | 10 | 2500 | 600 | 0.00398 | 0.368 |
| 4 | 20 | 500 | 400 | 0.00452 | 0.372 |
| 5 | 20 | 1500 | 600 | 0.00416 | 0.379 |
| 6 | 20 | 2500 | 200 | 0.00378 | 0.385 |
| 7 | 30 | 500 | 200 | 0.00423 | 0.374 |
| 8 | 30 | 1500 | 400 | 0.00365 | 0.388 |
| 9 | 30 | 2500 | 600 | 0.00308 | 0.396 |

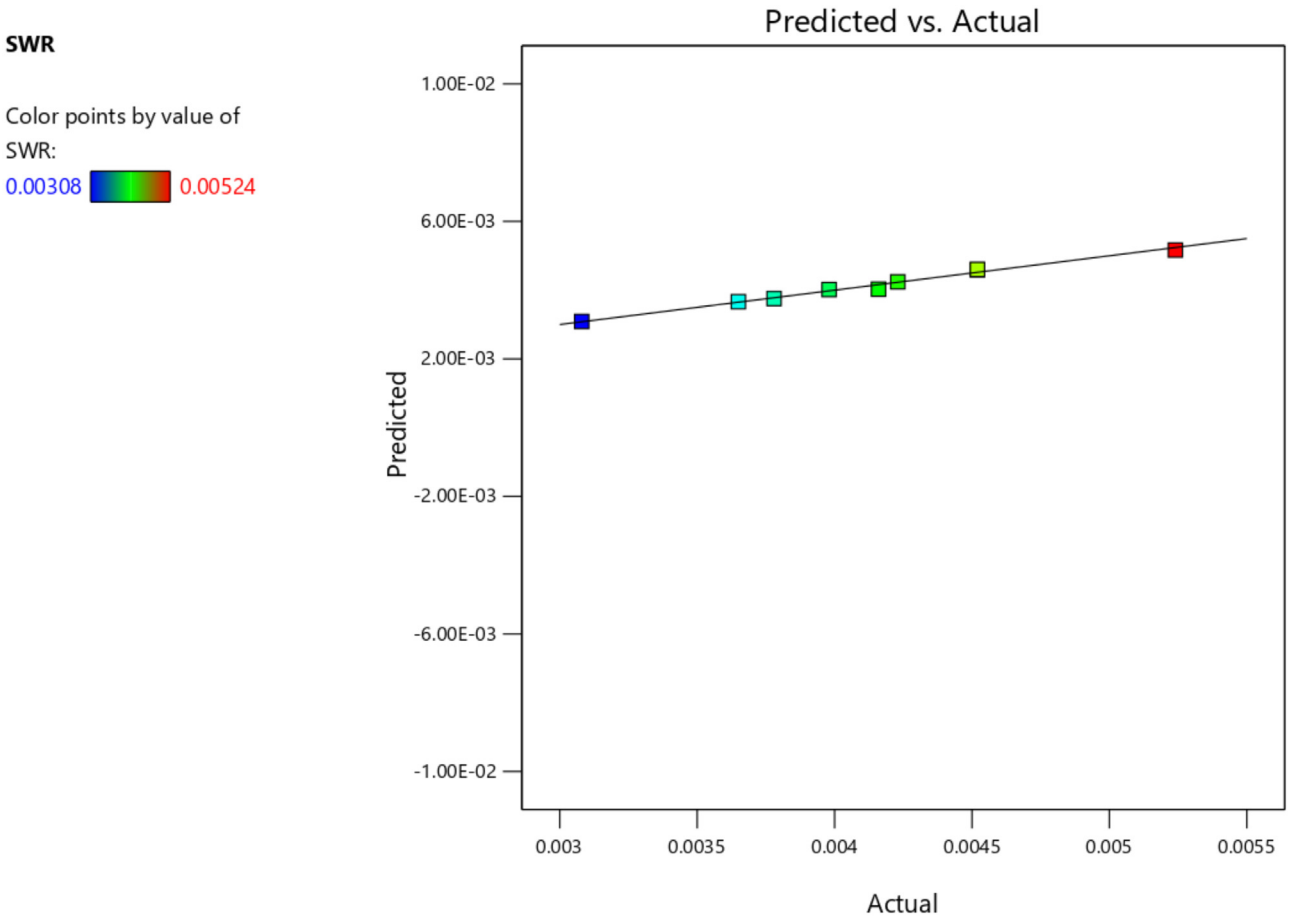


**Fig. 26.** Curve fitting for predicted versus actual values for SWR for AR2T6 specimen.

**Table 21.** Fit statistics of wear test for As cast specimen.

| | | | |
|---|---|---|---|
| Std. Dev. | 0.0001 | $R^2$ | 0.9877 |
| Mean | 0.0041 | Adjusted $R^2$ | 0.9803 |
| C.V.% | 2.09 | Predicted $R^2$ | 0.9654 |
| | | Adeq Precision | 36.1007 |

**Table 22.** Fit statistics of wear test for As cast specimen.

| | | | |
|---|---|---|---|
| Std. Dev. | 0.0057 | $R^2$ | 0.9292 |
| Mean | 0.3731 | Adjusted $R^2$ | 0.8867 |
| C.V.% | 1.53 | Predicted $R^2$ | 0.5604 |
| | | Adeq precision | 14.3373 |

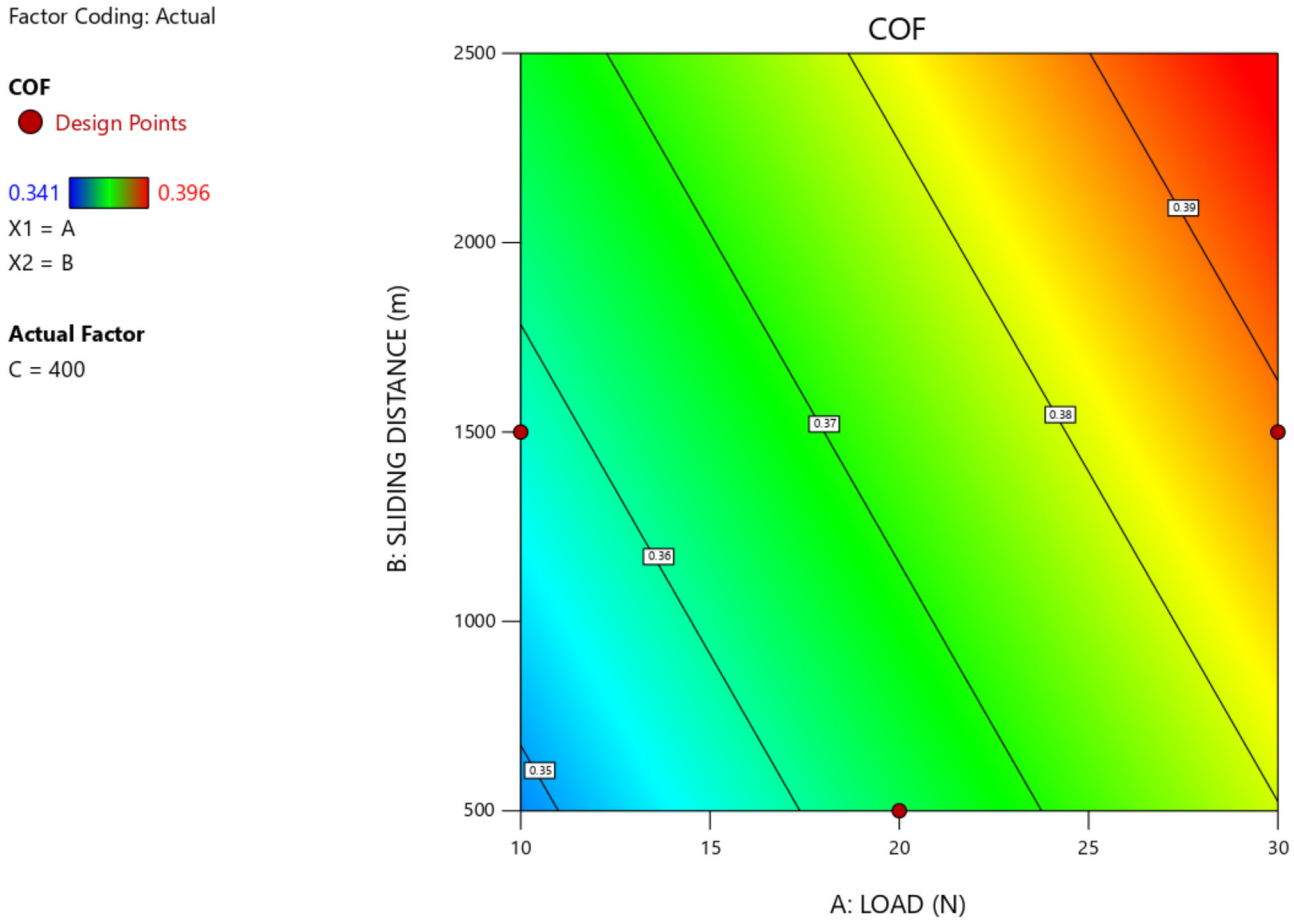


**Fig. 27.** Surface plot for variation of COF with load and sliding distance.

**Table 23.** ANOVA for SWR for AR2T6 specimens.

| Source | Sum of squares | df | Mean square | *F*-value | *p*-value | Remarks |
|---|---|---|---|---|---|---|
| Model | 2.988E-06 | 3 | 9.959E-06 | 133.62 | <0.0001 | Significant |
| A-LOAD | 1.288E-06 | 1 | 1.288E-06 | 172.82 | <0.0001 | |
| B-SLIDING DISTANCE | 1.013E-06 | 1 | 1.013E-06 | 135.90 | <0.0001 | |
| C-DISK ROTATION | 4.601E-08 | 1 | 4.601E-08 | 6.17 | 0.0555 | |
| Residual | 3.727E-08 | 5 | 7.453E-09 | | | |
| Cor Total | 3.025E-06 | 8 | | | | |

**Table 24.** ANOVA for COF for AR2T6 specimen.

| Source | Sum of Squares | df | Mean square | *F*-value | *p*-value | |
|---|---|---|---|---|---|---|
| Model | 0.0021 | 3 | 0.0007 | 21.86 | 0.0027 | Significant |
| A-LOAD | 0.0015 | 1 | 0.0015 | 45.02 | 0.0011 | |
| B-SLIDING DISTANCE | 0.0004 | 1 | 0.0004 | 11.14 | 0.0206 | |
| C-DISK ROTATION | 0.0000 | 1 | 0.0000 | 0.719 | 0.3680 | |
| Residual | 0.0002 | 5 | 0.0000 | | | |
| Cor Total | 0.0023 | 8 | | | | |

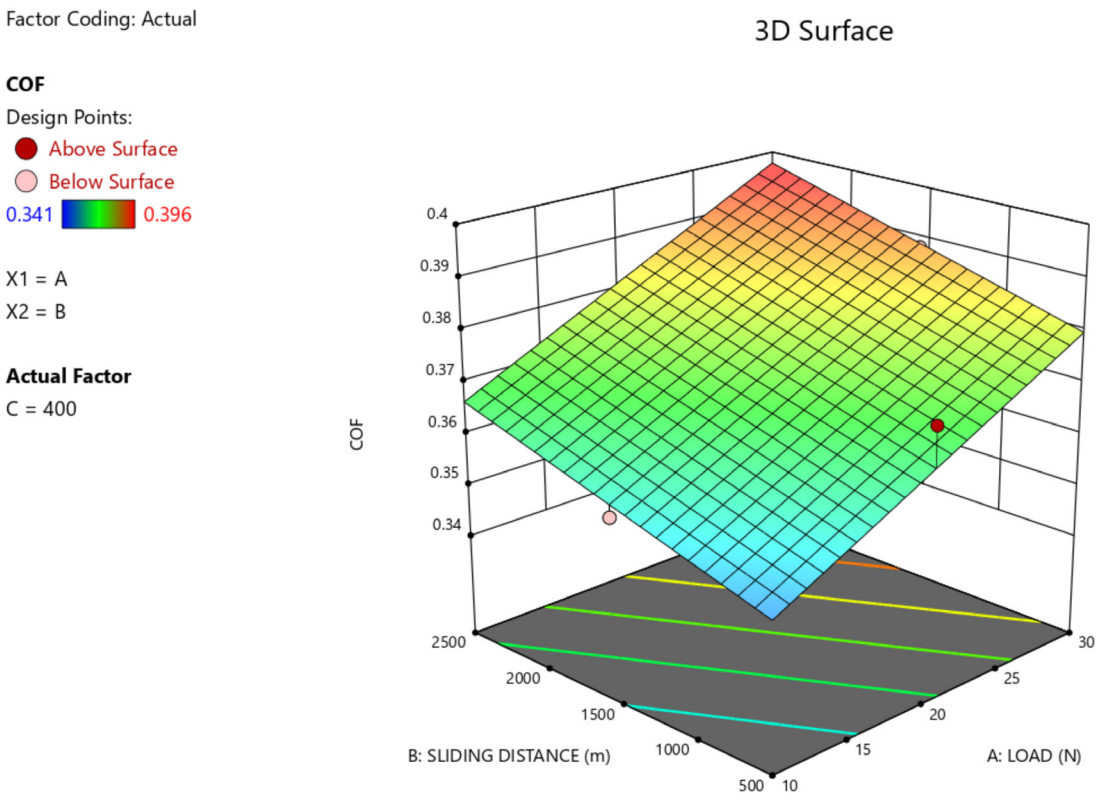


**Fig. 28.** 3D contour plot for variation of COF with load and sliding distance for AR2T6.

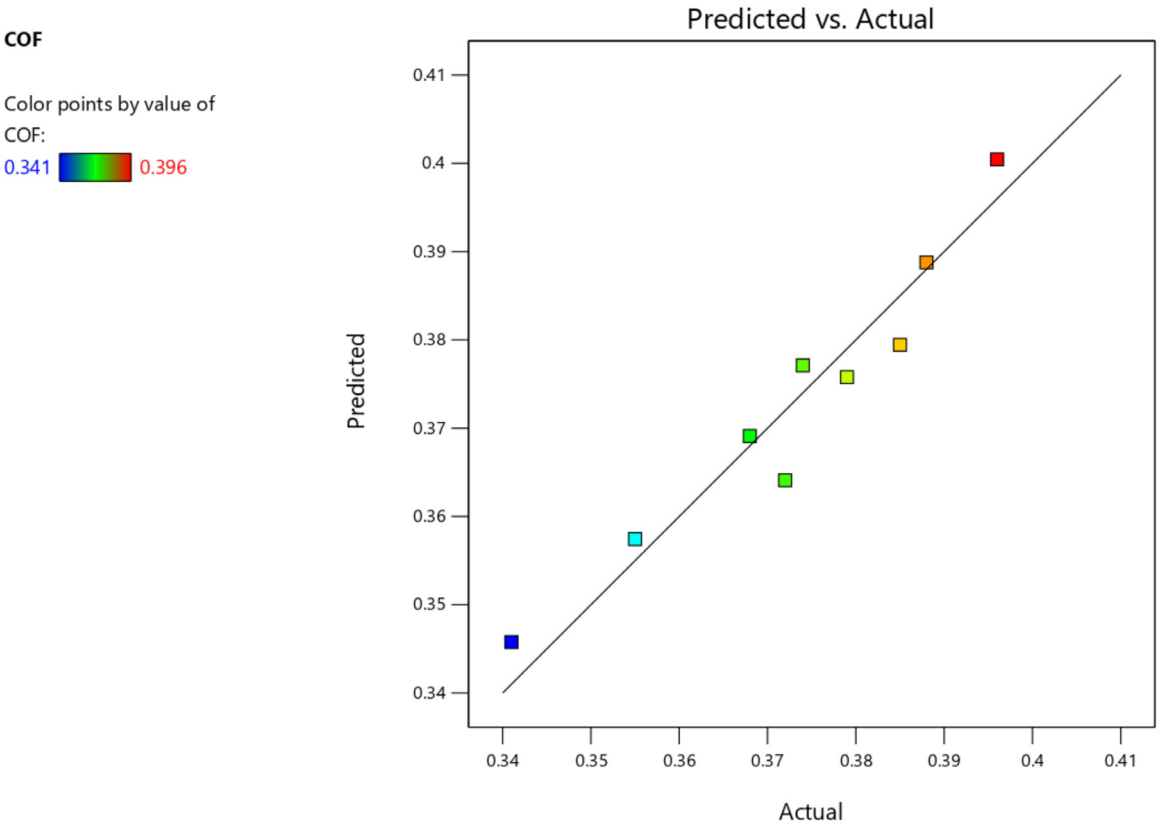


**Fig. 29.** Curve fitting for predicted versus actual values for COF for AR2T6 specimen.

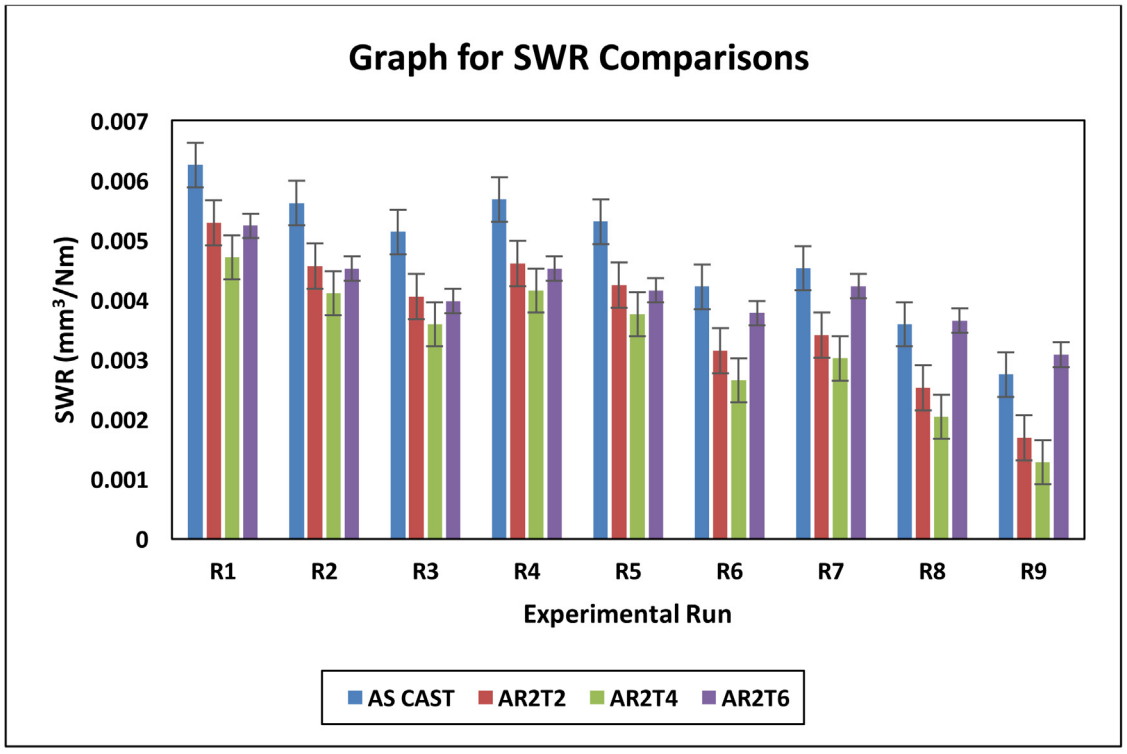


**Fig. 30.** Graph for SWR comparisons.

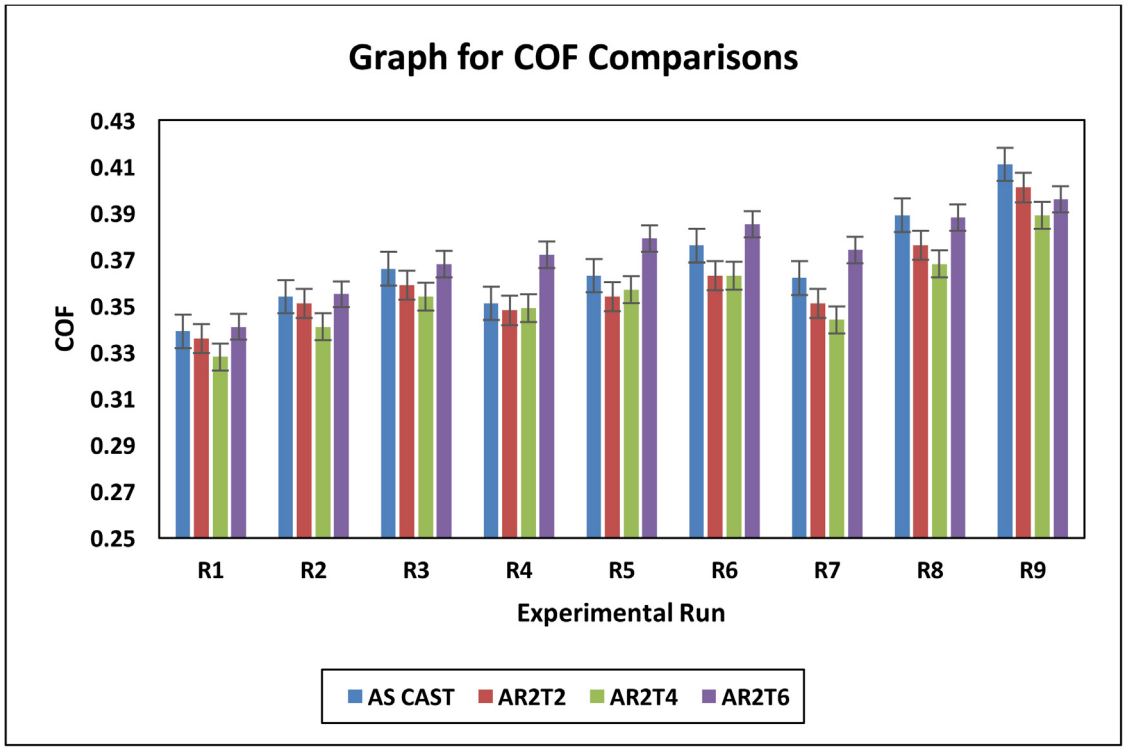


**Fig. 31.** Graphs for COF comparisons.


**Fig. 32.** Curve of coefficient of friction (COF) variation with test time for as cast specimen.

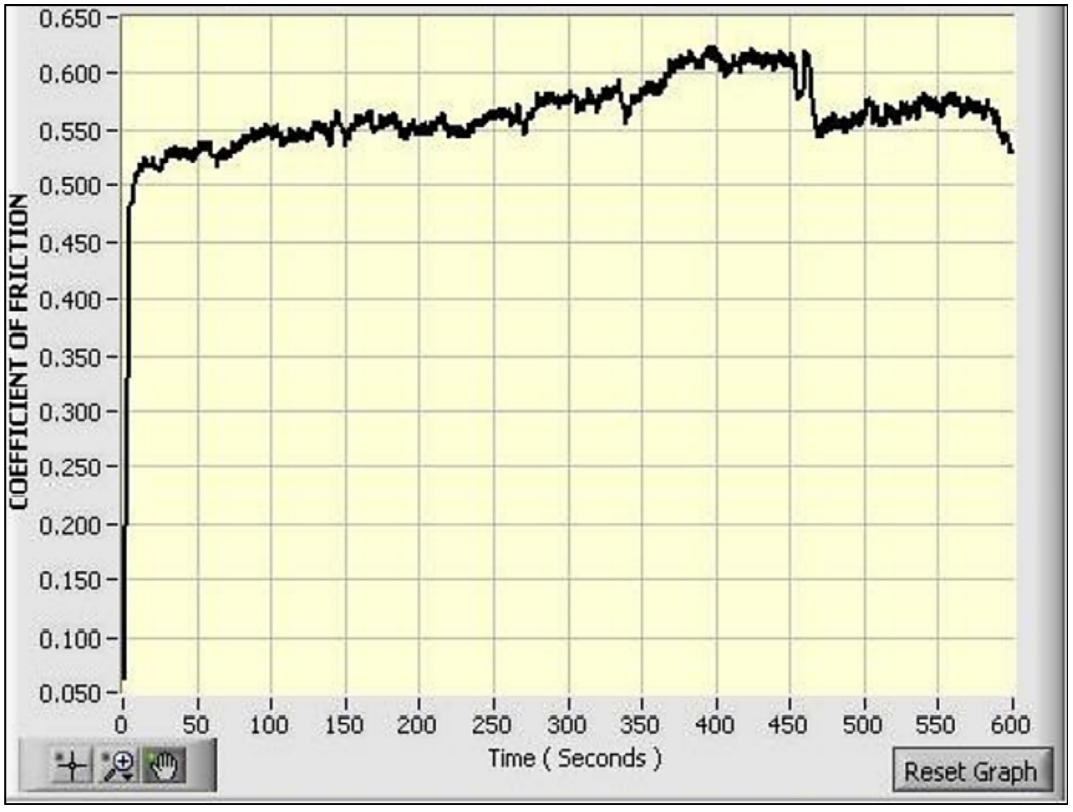


**Fig. 33.** Curve of coefficient of friction (COF) variation with test time for AR2T2 specimen.


**Fig. 34.** Curve of coefficient of friction (COF) variation with test time for AR2T4 specimen.

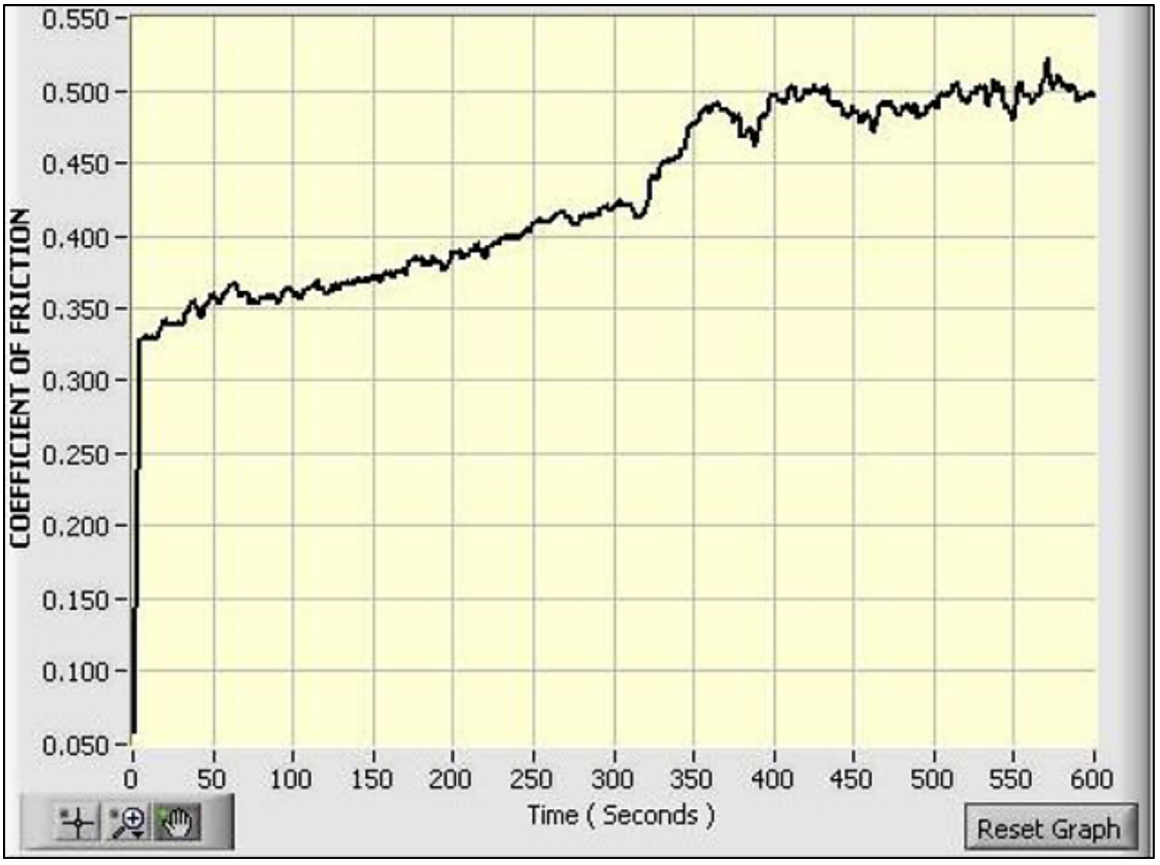


**Fig. 35.** Curve of coefficient of friction (COF) variation with test time for AR2T6 specimen.

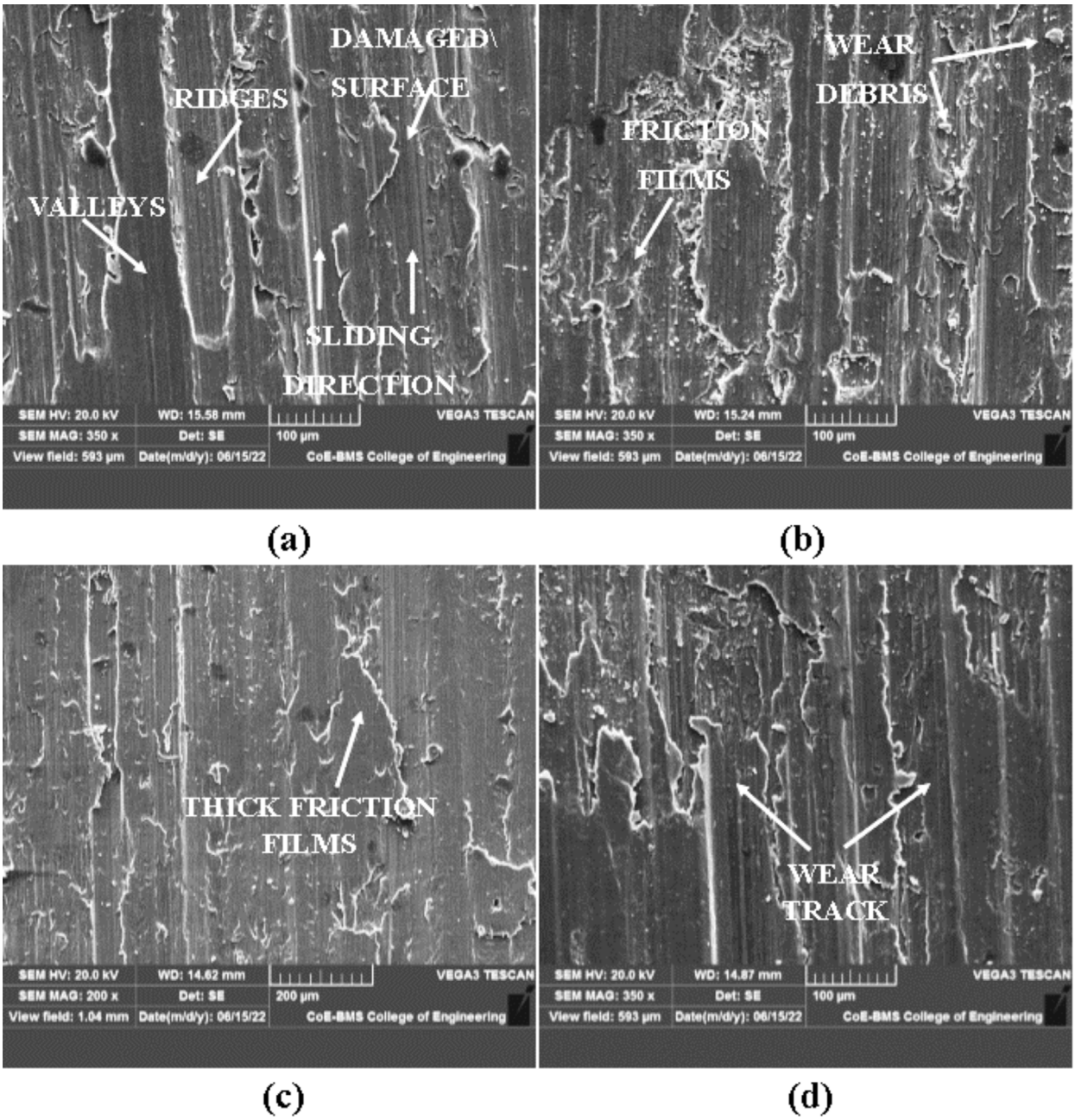


**Fig. 36.** SEM images of the worn surface of (a) As Cast (b) AR2T2 (c) AR2T4 (d) AR2T6 composite specimens.

## References

1. U.N. Kempaiah, N. Santhosh, D.H. Kumar, A.H. Chelgeri, P. Vishnu, S. Raorane, Characterization of high performance Al 5083/SiC/Fly Ash hybrid metal matrix composite for advanced aerospace applications, Int. J. Adv. Innov. Res. **3** (2015) 334–341
2. A.C. Gowda, D.P. Girish, N. Santhosh, A. Kumar, Study of wear characteristics of aluminium/B4C/CNT hybrid composites under the influence of controlled factors. Nano Trends A J. Nanotechnol. Appl. **18** (2016) 21–32
3. N. Santhosh, U.N. Kempaiah, S. Venkateswaran, Vibration mechanics of hybrid Al 5083/SiC/fly ash composite plates for its use in dynamic structures, J. Exp. Appl. Mech. **8** (2017) 11–18
4. N. Santhosh, U.N. Kempaiah, G. Sajjan, A.C. Gowda, Fatigue behaviour of silicon carbide and fly ash dispersion strengthened high performance hybrid Al 5083 metal matrix composites, J. Miner. Mater. Charact. Eng. **5** (2017) 274–287
5. N. Santhosh, U.N. Kempaiah, Vibration Characterization of SiC and fly ash dispersion strengthened aluminium 5083 composites, J. Aerosp. Eng. Technol. **7** (2017) 61–72

6. N. Santhosh, U.N. Kempaiah, R. Bhanupratap, Critically damped composite plates for structural applications in smart cities, in *Proceedings of the International Conference on Development of Smart Cities, Interface, Governance & Technology, Dr Ambedkar Institute of Technology*, Bangalore, Karnataka, India, 9–10 September 2016 (2016)
7. M. Sadashiva, H.K. Shivanand, M. Rajesh, N. Santhosh, Corrosion behavior of friction stir welded Al 6061 hybrid metal matrix composite plates, in *Proceedings of the International Conference on Advances in Mechanical Engineering Sciences (ICAMES-17)*, PESCE, Mandya, Karnataka, India, 21–22 April 2017 (2017)
8. N. Santhosh, U.N. Kempaiah, A.C. Gowda, S. Rao, G. Hebbar, Evaluation of corrosion mechanics of silicon carbide and fly ash reinforced hybrid aluminium metal matrix composites, in *Proceedings of the International Conference on Emerging Research in Civil, Aeronautical & Mechanical Engineering, ERCAM 2017*, Nitte Meenakshi Institute of Technology, Bengaluru, India, 21 July 2017 (2017), pp. 214–218.
9. K. Ramesha, P.D. Sudershanan, N. Santhosh, Mechanical and thermal characterization of friction stir weld joints of Al-Mg alloy, in *Proceedings of the International Conference on Emerging Trends in Mechanical Engineering (ETME)*, Mandya, India, 27–29 December 2017
10. N. Santhosh, U.N. Kempaiah, Effect of heat treatment and reinforcements on mechanical properties of aerospace grade Aluminium composites at elevated temperatures, in *Proceedings of the 2nd International Conference on Recent Research Emerging Trends in Mechanical & Civil Engineering, (ICRRETMCE-2018)*, REVA University, Bengaluru, Karnataka, India, 13–14 July 2018 (2018)
11. N. Santhosh, U.N. Kempaiah, Effect of silicon carbide and fly ash on characteristics of Aluminium matrix composites for improved dynamic performance, in *Proceedings of the Advanced Ceramics and Nano materials for Sustainable Development (ACeND-2018)*, CHRIST, Bangalore, Karnataka, India, 19–21 September 2018 (2018)
12. N. Santhosh, U.N. Kempaiah, G.S. Sunil, Novel aluminium–SiC–fly ash hybrid metal matrix composites: synthesis and properties, J. Aerosp. Eng. Technol. **7** (2017) 26–33
13. N. Santhosh, U.N. Kempaiah, Influence of ceramic particulate reinforcements on fly ash dispersion strengthened composites for aircraft structures, J. Aerosp. Eng. Technol. **7** (2017) 38–45.
14. T. Trzepiecinski, S.M. Najm, M. Sbayti, H. Belhadjsalah, M. Szpunar, H.G. Lemu, New advances and future possibilities in forming technology of hybrid metal–polymer composites used in aerospace applications, J. Compos. Sci. **5** (2021) 217
15. N. Santhosh, G.M. Khan, A. Dubey, S. Patel, A. Phookan, Fabrication and characterization of tensile properties of aluminum 5083/silicon carbide/fly ash composites for advanced engineering applications, J. Polym. Compos. **6** (2018) 6–9
16. F. Rana, D.M. Stefanescu, Friction properties of Al-l.5 Pet Mg/SiC particulate metal-matrix composites, Metall. Mater. Trans. A **20** (1989) 1564–1566
17. K.S. Al Rubaie, H.N. Yoshimura, D.B. Mello, Two-body abrasive wear of Al–SiC composites, Wear **233–235** (1999) 444–454
18. Y. Sahin, Optimization of testing parameters on the wear behaviour of metal matrix composites based on the Taguchi method, Mater. Sci. Eng. A **408** (2005) 1–8
19. I. Mokashi, A. Afzal, S.A. Khan, N.A. Abdullah, M.H. Bin Azami, R. Jilte, O.D. Samuel, Nusselt number analysis from a battery pack cooled by different fluids and multiple back-propagation modelling using feed-forward networks. Int. J. Therm. Sci. **161** (2020) 106738
20. N. Santhosh, N. Manjunath, H.R. Mahesh, Potentiodynamic corrosion characterization of hybrid aluminium composites for advanced engineering applications, Int. J. Eng. Adv. Technol. **9** (2020) 1434–1437
21. M. Akhtar, T. Sathish, V. Mohanavel, A. Afzal, K. Arul, M. Ravichandran, I. Rahim, S. Alhady, E. Bakar, B. Saleh, Optimization of process parameters in CNC turning of aluminum 7075 alloy using L27 array-based Taguchi method, Materials **14** (2021) 4470
22. M. Sadashiva, N.M. Siddeshkumar, J. Monica, M.R. Srinivasa, N. Santhosh, S. Praveenkumar, Hardness and impact strength characteristics of Al based hybrid composite FSW joints, Int. J. Vehicle Struct. Syst. **14** (2022) 13–17
23. M. Meignanamoorthy, M. Ravichandran, V. Mohanavel, A. Afzal, T. Sathish, S. Alamri, S. Khan, C. Saleel, Microstructure, Mechanical Properties, and Corrosion Behavior of Boron Carbide Reinforced aluminum alloy (Al-Fe-Si-Zn-Cu) matrix composites produced via powder metallurgy route, Materials **14** (2021) 4315
24. K. Ramesha, N. Santhosh, K. Kiran, N. Manjunath, H. Naresh, Effect of the process parameters on machining of GFRP composites for different conditions of abrasive water suspension jet machining, Web Sci. Scopus **9** (2019) 1–11
25. T. Sathish, A. Kaladgi, V. Mohanavel, K. Arul, A. Afzal, A. Aabid, M. Baig, B. Saleh, Experimental investigation of the friction stir weldability of AA8006 with zirconia particle reinforcement and optimized process parameters, Materials **14** (2021) 2782
26. N. Santhosh, B.A. Praveena, R. Jain, M. Abul Hasan, S. Islam, M. Amir Khan, A. Razak, Md Daniyal, Analysis of friction and wear of aluminium AA 5083/WC composites for building applications using advanced machine learning models, Ain Shams Eng. J. (2022) 102090
27. N. Santhosh, B.A. Praveena, A. Chandrashekar, V. Mohanavel, S. Raghavendra, D. Basheer, Wear behaviour of aluminium alloy 5083/SiC/fly ash inoculants based functional composites– optimization studies, Mater Res Express **9** (2022) 076513
28. G. Ravichandran, G. Rathnakar, N. Santhosh, R. Suresh, Wear characterization of HNT filled glass-epoxy composites using Taguchi's design of experiments and study of wear morphology, Compos. Theory Practice **20** (2020) 85–91
29. G. Ravichandran, G. Rathnakar, N. Santhosh, R. Thejaraju, Antiwear performance evaluation of halloysite nanotube (HNT) filled polymer nanocomposites, Int. J. Eng. Adv. Technol. **9** (2019) 3314–3321
30. M.R. Srinivasa, Y.S. Rammohan, M. Sadashiva, N. Santhosh, Effect of shock waves on the hardness of graphene reinforced aluminium composites, J. Polym. Compos. **8** (2020) 32–38
31. K. Ramesha, P.D. Sudersanan, N. Santhosh, S. Jangam, "Corrosion characterization of friction stir weld joints of dissimilar aluminum alloys, EAI/Springer Innov. Commun. Comput. (2021) https://doi.org/10.4108/eai.16-5-2020.2304097
32. K. Ramesha, P.D. Sudersanan, N. Santhosh, S. Jangam, Sustainable processing of dissimilar aluminium alloy joints

by friction stir welding, IOP Conf. Ser.: Mater. Sci. Eng. **1132** (2021) 012029
33. K. Ramesha, P.D. Sudersanan, N. Santhosh, S. Jangam, Design and optimization of the process parameters for friction stir welding of dissimilar aluminium alloys, Eng. Appl. Sci. Res. **48** (2021) 257–267
34. K. Ramesha, P.D. Sudersanan, P.K. Mahto, S.M. Ismail, A. C. Gowda, N. Santhosh, V. Umesh, Influence of heat treatment on the tensile and hardness characteristics of friction stir weld joints of dissimilar aluminium alloys, AIP Conf. Proc. **2421** (2022) 030001
35. K. Ramesha, P.D. Sudersanan, A.C. Gowda, N. Santhosh, S. Jangam, N. Manjunath, Friction stir welding of dissimilar aluminium alloys for vehicle structures, Int. J. Vehicle Struct. Syst. **14** (2022) 5–9
36. N. Santhosh, B.A. Praveena, H.V. Srikanth, S. Angadi, A. Gunge, M. Rudra Naik, G. Shankar, K. Ramesha, G. Ravichandran, Experimental investigations on static, dynamic, and morphological characteristics of bamboo fiber-reinforced polyester composites, Int. J. Polym. Sci. 2022 (**2022**) 1916877
37. N. Santhosh, B.A. Praveena, A. Chandrashekar, V. Mohanavel, S. Raghavendra, D. Basheer, Wear behaviour of aluminium alloy 5083/SiC/fly ash inoculants based functional composites – optimization studies, Mater. Res. Express **9** (2022) 076513
38. S. Nagaraja, K.U. Nagegowda, V.A. Kumar, S. Alamri, A. Afzal, D. Thakur, A.R. Kaladgi, S. Panchal, C.A. Saleel, Influence of the fly ash material inoculants on the tensile and impact characteristics of the aluminum AA 5083/7.5SiC composites, Materials **14** (2021) 2452
39. V. Bharath, V. Auradi, G.B.V. Kumar, M. Nagaral, M. Chavali, M. Helal, R. Sami, N. Aljuraide, J.W. Hu, A.M. Galal, Microstructural evolution, tensile failure, fatigue behavior and wear properties of Al2O3 reinforced Al2014 alloy T6 heat treated metal composites, Materials **15** (2022) 4244

**Cite this article as**: Niranjan Hugar, B. Venkata Narayana, Santhosh Nagaraja, Sunil Waddar, Effect of $TiO_2$ inoculants on the wear conduct of the aluminium AA 6061/red mud high performance hybrid composite, Manufacturing Rev. **10**, 4 (2023)